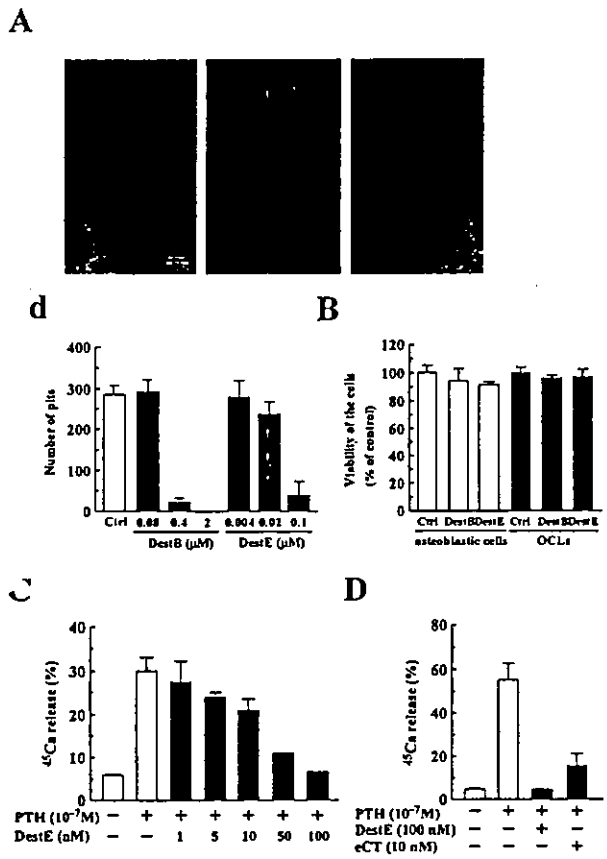

Fig. 2. Inhibitory effects of destruxins on the bone-resorbing activity of OCLs on dentine slices and in organ culture. Crude OCL preparations were placed on dentine slices (A) and 96-well culture plates (B) and cultured in the presence of 1% (v/v) DMSO (vehicle, Aa: Ctrl in Ad and B), 2 μM destruxin B (Ab, DestB in B) or 0.1 μM destruxin E (Ac, DestE in B). Osteoblastic cells cultured on 96-well culture plates (B) were cultured in the presence of 1% (v/v) DMSO (vehicle; Ctrl) or destruxins (100 μM). After culture for 24 h, the slices were stained with Mayer's hematoxylin (A), the OCLs were stained for TRAP (B) and the osteoblastic cells were incubated with crystal violet (B). The numbers of pits (Ad) and TRAP-itive multinucleated cells (B) were counted. The absorbance resulting ..n the crystal violet incorporated into the cytoplasm of living cells was measured at 595 nm (B). ^{45}Ca-prelabeled bones were cultured for 72 h with or without the indicated concentrations of destruxin E or eel calcitonin in the presence of PTH (10^{-7} M) (C,D). At the end of the culture period, bones were extracted in 0.1 N HCl. The radioactivity in media and bone extracts was determined. The bone-resorbing activity was expressed as the percentage of incorporated ^{45}Ca that was released into the medium. Data are expressed as the mean ± SD of four cultures. Bar = 100 μm.

Destruxins did not affect early differentiation of progenitor cells into TRAP-positive mononuclear osteoclasts, or their fusion into multinucleated osteoclasts

We next examined whether or not an effect of destruxins on osteoclastic differentiation was involved in the inhibition of pit formation by OCLs. In this study, we examined the effect of destruxins on the early differentiation of the TRAP-negative osteoclast precursor cells into pOCs (Fig. 3A) and on the fusion of pOCs to form OCLs (Fig. 3B). The osteoclast precursor cells prepared from bone marrow cells by M-CSF were cultured in the presence of M-CSF and sRANKL for 48 h and with destruxins for the last 24 h. Destruxins did not affect pOC formation at the concentrations that inhibited pit formation by OCLs (Fig. 3A). When pOCs, prepared from cocultures of bone marrow cells and calvarial osteoblastic cells, were cultured in the presence of M-CSF and sRANKL for 24 h, OCLs were formed by fusion of the pOCs. Destruxins did not inhibit the fusion of pOCs into OCLs at the concentrations that inhibited pit formation by OCLs (Fig. 3B). These results also suggest that destruxins inhibit pit formation by affecting the bone-resorbing function of OCLs.

Destruxins specifically inhibit the polarization process of osteoclasts

It is generally recognized that polarization of osteoclasts is an essential event to initiate bone resorption [1]. Since actin rings are believed to be one of the markers of polarized osteoclasts [3], we examined whether or not an effect of destruxins on actin ring formation was involved in the inhibition of pit formation by OCLs. When OCLs were placed on plastic plates, approximately 70% of OCLs possessed a clear cytoplasm, smooth periphery, and actin rings within 6 h (Figs. 4A, B, and D). The time course of actin ring formation was correlated to that of pit formation (Figs. 4B and D). However, OCLs formed no actin rings in cultures with destruxins (Fig. 4B). In these OCLs, F-actins were distributed throughout the cytoplasm in the cells (Figs. 4Dd and f). In the presence of destruxins, the cytoplasm of OCLs was foamy rather than clear, and the cell periphery was irregular rather than smooth (Figs. 4A and D). Furthermore, in the cultures with destruxins, no pit formation by OCLs on dentine slices was observed (Fig. 4D). These results suggest that destruxins inhibit polarization of osteoclasts and the effects of destruxins on the morphologies of OCLs are involved in the inhibition of pit formation.

Destruxins specifically disrupt morphological structures in polarized OCLs

To examine the effect of destruxins on polarized osteoclasts, polarized OCLs on plastic plates were cultured with destruxins. As shown in Fig. 5, destruxins induced morphological changes in the presence of osteoblastic cells in a dose-dependent manner (DestB, 0.2–1 μM; DestE, 0.01–0.05 μM). The effects of 0.0625–0.25 μM destruxin E were equivalent to those of 1.25–5 μM destruxin B, and the ED_{50} value of destruxin E was lower than that of destruxin B (ED_{50}; DestB = 0.4 μM; DestE = 0.012 μM). The morphology of more than 90% of OCLs was changed by 0.6 μM destruxin B or 0.03 μM destruxin E. The same effects were also observed in the absence of osteoblastic cells (Fig. 6). Furthermore, F-actin staining showed that destruxins disrupted actin rings in OCLs (Figs. 6b,d, and f) without affecting the structure of F-actin stress fibers in osteoblastic cells (data not shown). The actin rings were completely disrupted by 2 μM destruxin B or 0.1 μM

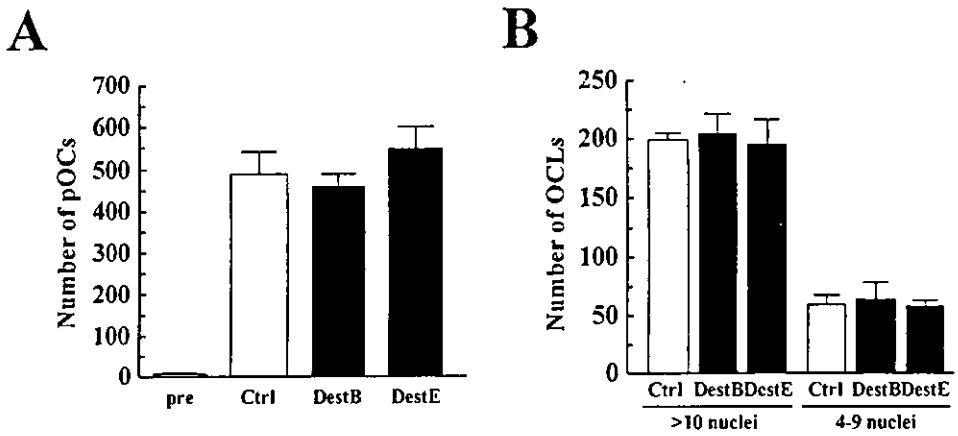

Fig. 3. Effect of destruxins on the differentiation of TRAP-negative osteoclast precursor cells into OCLs. TRAP-negative osteoclast precursor cells (A) and pOCs (B) were cultured for 24 and 48 h on 96-well culture plates in the presence of M-CSF (20 ng/ml) and sRANKL (100 ng/ml), respectively. For the last 24 h, the cells were cultured with 0.02% (v/v) DMSO (vehicle; Ctrl), 2 μM destruxin B (DestB), or 0.1 μM destruxin E (DestE). After the culture, the cells were fixed and stained for TRAP, and then the number of pOCs (A) and OCLs with more than 4 nuclei (B) were counted. Data are expressed as the mean ± SD of four cultures.

destruxin E within 24 h, and F-actins were distributed throughout the cytoplasm in the cells (Figs. 6b,d, and f). These results suggest that destruxins directly induce the morphological changes and disruption of actin rings in polarized OCLs.

Effects of destruxins on the morphological changes in polarized OCLs and on bone-resorbing activity are reversible

To characterize the behavior of destruxins against the morphologies in osteoclasts, we observed the morphologies in OCLs cultured with destruxins (DestB, 2 μM; DestE, 0.1 μM) at each time point. As shown in Fig. 7A and B, the percentage of OCLs with a clear cytoplasm and smooth periphery decreased with time after culture with destruxins. After culture with destruxins for 12 h, the OCLs in the cultures showed no actin rings (data not shown). Culture with 2 μM destruxin B took 1 h to induce morphological changes in more than 90% of OCLs in the culture, whereas culture with 0.1 μM destruxin E took 8 h. We continuously examined what happened to the morphologies in OCLs after removal of the destruxins from the culture media. The morphologies of OCLs exhibited by culture with destruxins were not present at 24 h after removing the destruxin-containing culture media, successively washing the cells with fresh media, and culturing with fresh media (Figs. 7A and B). The percentage of OCLs with a clear cytoplasm and smooth periphery increased with time after removal of the destruxins. However, the percentage did not increase over the examination period when the destruxins were not removed (data not shown). Although OCLs cultured with destruxin E required more time for the transition of morphology compared to OCLs cultured with destruxin B before and after removal of the destruxins, no rapid transition, but rather osteoclastic cell death, was induced when OCLs were cultured with 1 μM destruxin E (data not shown). OCLs cultured with destruxins showed actin rings at 24 h after removal of the destruxins (data not shown). We successively examined whether the bone-resorbing function was exerted in the OCLs cultured with destruxins, after removal of the destruxins. When the OCLs cultured with destruxins were cultured again in fresh media after removal of the destruxins, the number and size of pits were increased compared to those before the removal (Fig. 7C). Although the number of pits was not increased by the removal of DMSO in the control culture, the size of each pit was increased (Figs. 7Ca,b, and e). These results suggest that destruxins reversibly induce morphological changes in polarized OCLs, resulting in reversible inhibition of bone resorption.

Destruxin B reversibly induces disorders of structures and distribution of V-ATPase in OCLs at the ultrastructural level

To investigate the effects of destruxins on the morphology of OCLs in detail, we observed cell structures of OCLs on dentine slices at the ultrastructural level. When OCLs were placed on dentine slices, more than 90% of OCLs showed a polarized cytoplasmic organization, with clear zones and ruffled borders (Figs. 8a, b, and 9a). However, OCLs cultured with 2 μM destruxin B for 2 h showed no prominent ruffled borders, but rather broad clear zone-like structures facing the dentine slices (Figs. 8c, d, and 9b). Among the OCLs cultured with 2 μM destruxin B (n = 20), 75% of OCLs showed no ruffled borders and clear zones, and the other 25% showed irregular ruffled borders and clear zones. Characteristically, many large vacuoles were accumulated in the cytoplasm just proximal to the broad clear zones in the OCLs cultured with destruxin B (Figs. 8c, and d). However, when the OCLs cultured with destruxin B

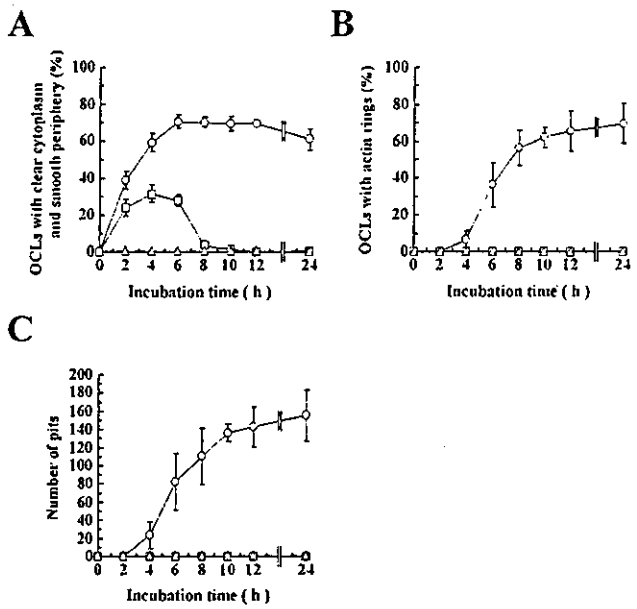

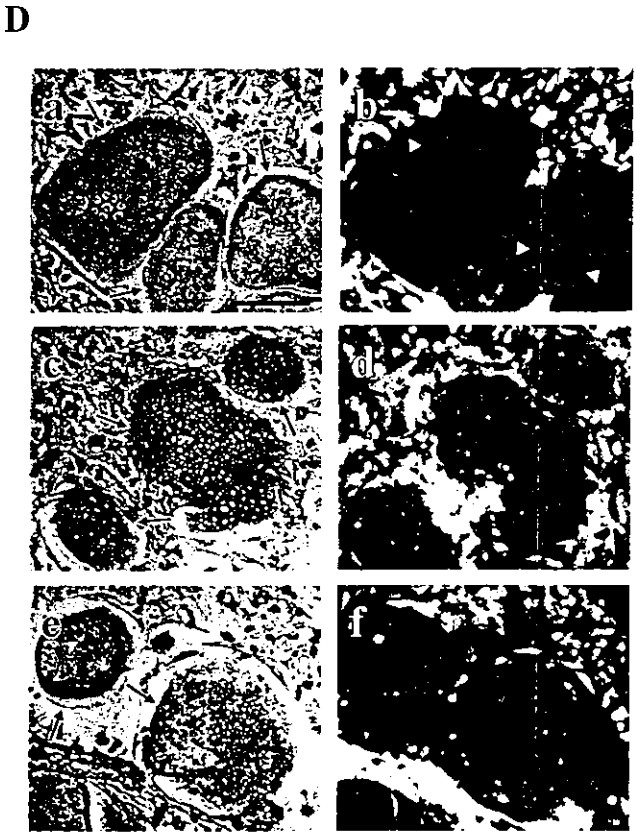

Fig. 4. Effect of destruxins on the polarization process of OCLs. OCLs with osteoblastic cells harvested from cocultures were cultured again in 96-well culture plates (A.B.D) or on dentine slices (C) in the presence of 1% (v/v) DMSO (vehicle: circles in A–C, Da.b), 2 μM destruxin B (triangles in A–C, Dc.d), or 0.1 μM destruxin E (squares in A–C, De.f) for the indicated periods. After the culture, the cells and slices were stained for TRAP (A.B.D) and with Mayer's hematoxylin (C), respectively. The numbers of OCLs with a clear cytoplasm and smooth periphery (A), OCLs with actin rings (B), and pits (C) were counted. OCLs cultured for 6 h were further stained by Alexa488-conjugated phalloidin (Db.d.f) after the staining for TRAP (Da.c.e). Data are expressed as the percentage of the total number of OCLs (A.B) or as a number (C) in the culture (mean ± SD; n = 4). Arrows: TRAP-positive multinucleated cells. Arrowheads: actin rings. Bar = 100 μm.

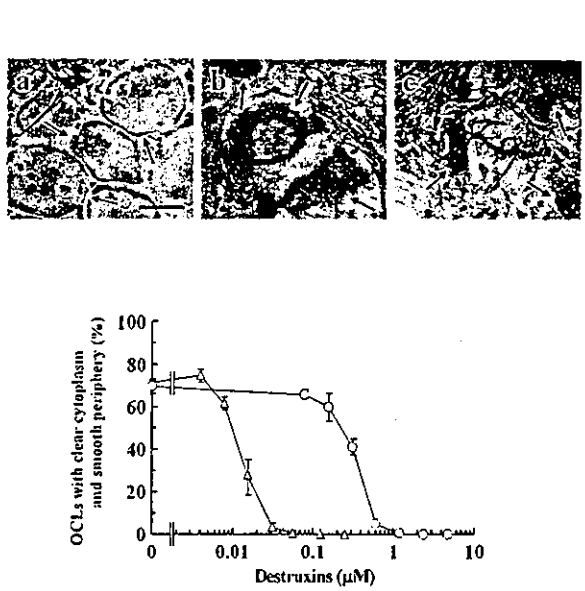

Fig. 5. Effects of destruxins on the morphology of polarized OCLs in the presence of osteoblastic cells. Crude OCLs prepared from cocultures were cultured with or without destruxins for 24 h on 96-well culture plates [1% DMSO (vehicle); Aa, destruxin B; Ab, circles in B; destruxin E; Ac, triangles in B]. After the culture, the cells were stained for TRAP (A) and the number of OCLs with a clear cytoplasm and smooth periphery were counted (B). Data are expressed as the percentage of the total number of OCLs in the culture (mean ± SD; n = 4). Arrows: TRAP-positive multinucleated cells. Bar = 100 μm.

were cultured again in fresh media without destruxin B, the OCLs showed the ruffled border and clear zone structures at 4 h after the reculture (Figs. 8e and 9c). Among these OCLs recultured without destruxin B (n = 11), 81.8% of OCLs showed ruffled borders and clear zones, and the other 18.2% also formed irregular ruffled borders and clear zones. Throughout the experiment, neither necrotic nor apoptotic cell death were observed in any destruxin B-treated OCLs (data not shown). These results suggest that destruxins induce the structural disorders of osteoclasts placed on bone.

We also examined the V-ATPase localization in the destruxin B-treated OCLs by immunocytochemistry. As reported previously [6,7], immunogold particle deposition for V-ATPase was observed along the ruffled borders in OCLs in the control culture (Fig. 9a). However, among the OCLs cultured with 2 μM destruxin B for 2 h (n = 5), 60% of OCLs showed no immunogold particles along the plasma membrane facing the dentine slices (Fig. 9b). Alternatively, these OCLs showed immunogold particles scattered throughout the cytoplasm and the particles along the limiting membranes of some vacuoles that were lucent under an electron microscope (Fig. 9b). However, when the OCLs cultured with destruxin B were cultured again in fresh media without destruxin B, immunogold particles along the plasma membrane were observed in the OCLs at 4 h after the reculture (Fig. 9c). Among the OCLs recultured without destruxin B (n = 6), 66.7% of the OCLs showed immunogold particles along the plasma membrane. These results

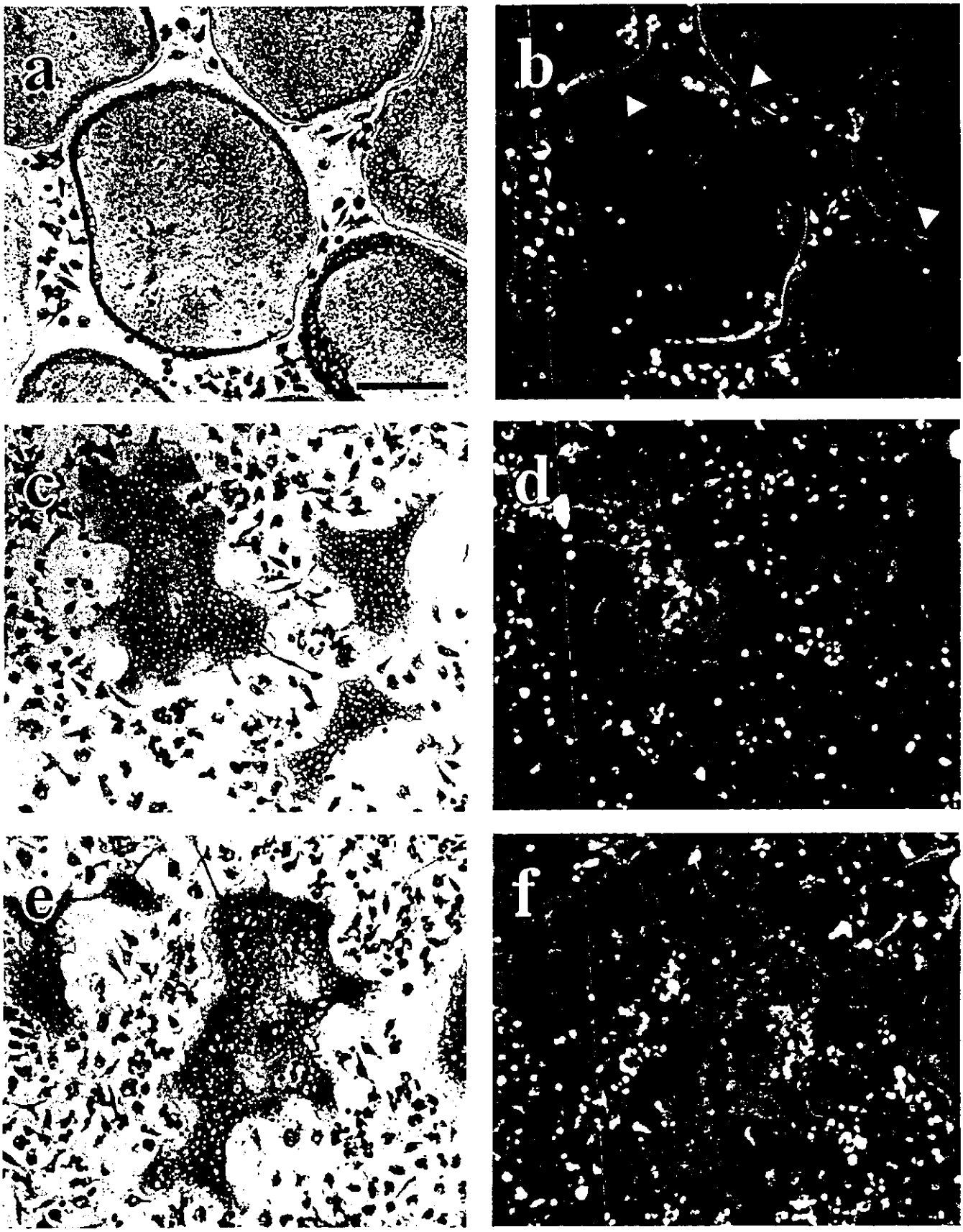

Fig. 6. Effects of destruxins on the morphology of polarized OCLs in the absence of osteoblastic cells. OCL preparations prepared from pOCs culture were cultured with 0.02% (v/v) DMSO (vehicle; a,b), 2 μM destruxin B (c,d), or 0.1 μM destruxin E (e,f) for 24 h in the presence of M-CSF (20 ng/ml) and sRANKL (100 ng/ml) on 96-well culture plates. Light micrographs (a,c,e) and fluorescent micrographs (b,d,f) were prepared from OCLs stained for TRAP and further stained by Alexa488-conjugated phalloidin. Arrowheads: actin rings. Bar = 100 μm.

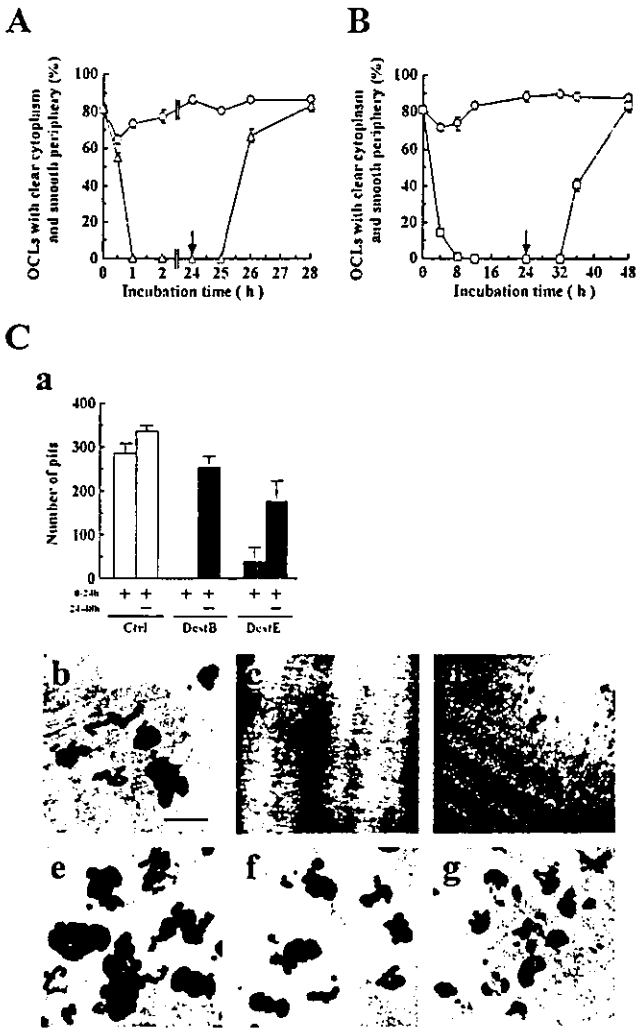

Fig. 7. Reversible changes of the morphology and pit-forming activity in OCLs cultured with destruxins. Crude OCL preparations placed on 96-well culture plates (A,B) and dentine slices (C) were cultured in the presence of 1% (v/v) DMSO (vehicle) (circles in A and B, Ctrl in C, Cb,e), 2 μM destruxin B (triangles in A, DestB in C, Cc,f), or 0.1 μM destruxin E (squares in B, DestE in C, Cd,g) for the indicated periods. In some cultures, the culture medium was replaced with fresh medium without DMSO or destruxins (arrows in A and B) and the cells were further cultured for the indicated periods. After the culture, the OCLs were fixed and stained for TRAP (A,B) and the slices were stained with Mayer's hematoxylin (C). The numbers of OCLs with a clear cytoplasm and smooth periphery or pits were counted. Data are expressed as the percentage of the total number of OCLs (A,B) or as a number (C) in the culture (mean ± SD; $n = 4$). Bar = 100 μm.

suggest that destruxins induce disorder of the V-ATPase localization in osteoclasts.

Discussion

In the present study, we found that destruxins inhibit the bone-resorbing activity of OCLs. Destruxins are fungal secondary metabolites and were first isolated as substances toxic to insects and plants [13,14]. In addition to their insecticidal and phytotoxic activities [18–20], they were demonstrated to show anti-tumor [21,22] and anti-viral [23–25] activities. In this paper, we have reported the anti-resorptive activities of destruxins for the first time. Destruxins inhibited bone resorption by OCLs without affecting their survival. However, destruxins inhibited neither the early differentiation of progenitor cells into pOCs nor the fusion of pOCs into OCLs. These results suggest that destruxins inhibit bone resorption by specifically affecting the bone-resorbing function of osteoclasts.

As has been shown in previous studies [11,26–28], OCLs prepared from the coculture system were more than 150 μm in diameter. These OCLs also possessed clear cytoplasm and smooth periphery in addition to actin rings [11,17,26–28]. When OCLs were cultured with the concentrations of destruxins that inhibited bone resorption, the cytoplasm of OCLs was foamy rather than clear, the periphery was irregular rather than smooth, and F-actins were distributed throughout the cytoplasm. Such OCLs with no actin rings also exhibited no pit-forming activity as well as osteoclasts whose actin rings were disrupted by various inhibitors [11,28–30]. Destruxins also disrupted actin rings in polarized OCLs on plastic plates in the absence of osteoblastic cells, and ruffled borders and clear zones in polarized OCLs on dentine slices. When destruxins were added to or removed from the culture media, the transition of the percentage of OCLs with a clear cytoplasm and smooth periphery and that of OCLs with ruffled borders and clear zones were similar to each other. When the OCLs cultured with destruxins were cultured again in fresh media after removal of the destruxins, the number and size of pits were increased compared to those before the removal. These results suggest that destruxins inhibit the bone-resorbing activity of osteoclasts by directly inducing a disorder of the morphological structures in polarized osteoclasts. The properties of destruxins shown in this paper (e.g., specificity to polarized OCLs and an anti-resorptive effect of destruxin E as strong as that of calcitonin) encourage us to develop them as therapeutic agents for the treatment of osteoporosis. We have not investigated the effects of destruxins in vivo, because we have only a small amount of destruxins in our laboratory, but it will be a worthwhile study.

The concentration of destruxin E that affected the morphologies in OCLs was 30-fold lower than that of destruxin B at the point of ED_{50}. However, OCLs cultured with destruxin E required more time for the transition of morphology compared to OCLs cultured with destruxin B before and after removal of the destruxins. As shown in Fig. 1, the structure of the hydroxy acid moiety in the basic structure will determine the biological effect of each destruxin. The insecticidal effect of destruxin E is also exhibited at lower concentrations than those of destruxin B [31], and the concentration of destruxin E required to inhibit the proliferation of leukemic cells is about 30-fold lower than that of destruxin A or destruxin B (their IC_{50} values are 0.33, 11.7, and 9.4 μg/ml, respectively) [25]. This similarity suggests that the action of destruxins on polarized OCLs may derive from the same mechanism involved in the other activities. A

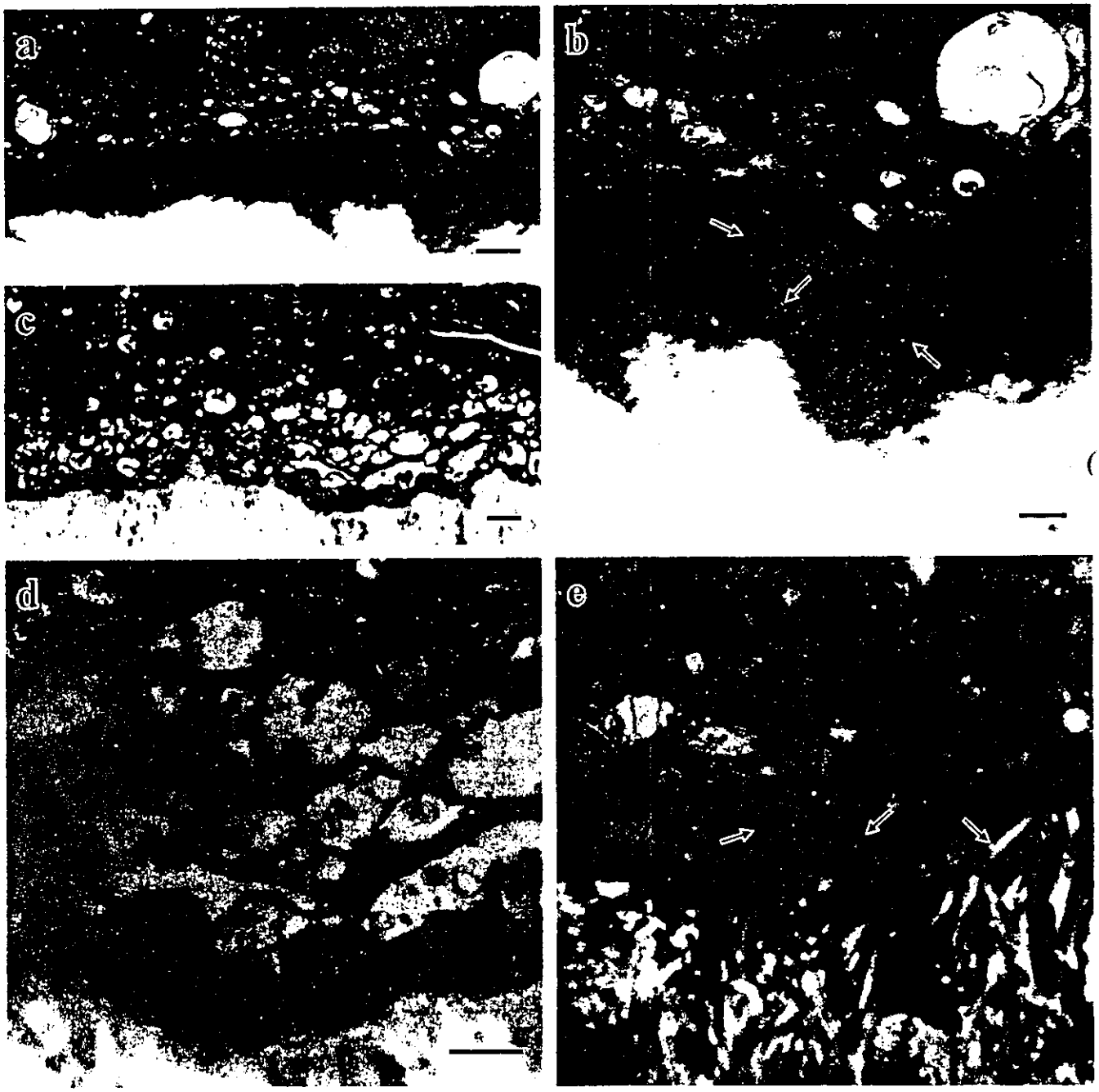

Fig. 8. Effect of destruxin B on the ultrastructure in OCLs on dentine slices. Crude OCL preparations were placed on dentine slices, cultured for 2 h in the absence (a,b) or presence of 2 μM destruxin B (c,d), and then fixed. Some of the OCLs cultured with destruxin B were further cultured for 4 h in fresh medium without it (e) and then fixed. After fixation, ultrathin sections of OCLs were prepared and then examined under an electron microscope. Arrows: ruffled borders. CZ: clear zones. Bars = 1 μm (a,b), 500 nm (c–e).

few studies have reported that destruxins inhibit the hydrolytic activity of V-ATPase [32,33] and concluded that this activity was responsible for the inhibition of CTL-mediated cytotoxicity and lipid accumulation in macrophages [34,35]. These reports indicate that destruxins inhibit the acidification by V-ATPase of intracellular organelles such as lysosomes and endosomes. At concentrations that affected the morphology of OCLs, destruxins did not inhibit the acidification of osteoclastic intracellular organelles as evidenced by acridine orange staining (data not shown). Destruxins are also known to induce the gene expression for erythropoietin production in the epo-3 line [36], to exert an inotropic effect on mammalian hearts [37], to increase intracellular calcium levels, and to increase the phosphorylation levels of intracellular proteins in lepidopteran cell lines [18,31]. The possibility of calcium ion involvement in the behaviors of destruxins on OCLs was not excluded by the present study. To date, the involvement of several signal-transducing mol-

ecules in the regulation of osteoclast function has been demonstrated by low-molecular-weight compounds (RGD peptides, herbimycin, wortmannin, statins, etc.), e.g., RGD sequence [38,39], $p60^{c\text{-}src}$ tyrosine kinase (c-Src) [40,41], phosphatidylinositol-3 kinase (PI3K) [26,27], small GTP-binding proteins [28–30,42,43], cAMP, and PKA [9–11]. In the present study, we indicated that the behavior of destruxins on OCLs was similar to that of calcitonin, in that bone resorption by OCLs was inhibited without affecting their survival. However, the morphologies of OCLs exhibited by culture with destruxins were present during the experiment when the destruxins were not removed (data not shown). The involvement of CTR and PKA in the behavior of destruxins was also not determined in the present study. Further studies will be required to determine whether or not destruxins affect osteoclasts by the same mechanism as calcitonin. The specific activities of destruxins on polarized OCLs will contribute to the elucidation of the relationship between polarization and the function of osteoclasts. Since the molecular targets of destruxins in mammalian cells remain to be elucidated, further studies will be required to explain the detailed physiological action mechanisms of destruxin in osteoclasts as well as in other mammalian cells.

It is important to identify the target molecules and action mechanism of destruxins, and to elucidate how destruxins affect the morphological structures and bone-resorbing activity of functional osteoclasts. These worthwhile studies are now in progress. Knowledge of the specific properties of destruxins in relation to functional OCLs will be useful for elucidating the processes of polarization and expression of osteoclast function, resulting in the provision of novel information and new therapeutic targets for metabolic bone disorders.

Acknowledgments

We thank Dr. A. Takatsuki (The Institute of Physical and Chemical Research, Saitama, Japan) and Dr. K. Hasumi (Tokyo University of Agriculture and Technology, Tokyo, Japan) for the generous gifts of destruxins. This work was partly supported by Grants-in-Aid for Scientific Research (C) (14560079) from the Ministry of Education, Culture, Sports, Science, and Technology of Japan.

Fig. 9. Effect of destruxin B on V-ATPase localization in OCLs on dentine slices. Crude OCL preparations were placed on dentine slices, cultured for 2 h in the absence (a) or presence of 2 μM destruxin B (b), and then fixed. Some of the OCLs cultured with destruxin B were further cultured for 4 h in fresh medium without it (c), and then fixed. Ultrathin sections of OCLs were prepared, incubated with rabbit anti-V-ATPase antibodies and then with goat anti-rabbit IgG conjugated with 10-nm colloidal gold particles. Some of the immunogold particles, which indicate V-ATPase, are indicated by arrow-heads. Arrows: ruffled borders. Bar = 500 nm.

References

[1] Suda T, Takahashi N, Martin TJ. Modulation of osteoclast differentiation. Endocr Rev 1992;13:66–80.

[2] Baron R. Molecular mechanisms of bone resorption by the osteoclast. Anat Rec 1989;224:317–24.

[3] Suda T, Nakamura I, Jimi E, Takahashi N. Regulation of osteoclast function. J Bone Miner Res 1997;12:869–79.

[4] Duong LT, Lakkakorpi P, Nakamura I, Rodan GA. Integrins and signaling in osteoclast function. Matrix Biol 2000;19:97–105.

[5] Rodan SB, Rodan GA. Integrin function in osteoclasts. J Endocrinol 1997;154:S47–56.

[6] Väänänen HK, Karhukorpi EK, Sundquist K, Wallmark B, Roininen I, Hentunen T, Tuukkanen J, Lakkakorpi P. Evidence for the presence of a proton pump of the vacuolar H^+-ATPase type in the ruffled borders of osteoclasts. J Cell Biol 1990;111:1305–11.

[7] Mattsson JP, Skyman C, Palokangas H, Väänänen HK, Keeling DJ. Characterization and cellular distribution of the osteoclast ruffled membrane vacuolar H^+-ATPase B-subunit using isoform-specific antibodies. J Bone Miner Res 1997;12:753–60.

[8] Body JJ. Calcitonin for the long-term prevention and treatment of postmenopausal osteoporosis. Bone 2002;30:75S–9S.

[9] Holtrop ME, Raisz LG, Simmons HA. The effects of parathyroid hormone, colchicine, and calcitonin on the ultrastructure and the activity of osteoclasts in organ culture. J Cell Biol 1974;60:346–55.

[10] Lerner UH, Ransjo M, Klaushofer K, Horandner H, Hoffmann O, Czerwenka E, Koller K, Peterlik M. Comparison between the effects of forskolin and calcitonin on bone resorption and osteoclast morphology in vitro. Bone 1989;10:377–87.

[11] Suzuki H, Nakamura I, Takahashi N, Ikuhara T, Matsuzaki K, Isogai Y, Hori M, Suda T. Calcitonin-induced changes in the cytoskeleton are mediated by a signal pathway associated with protein kinase A in osteoclasts. Endocrinology 1996;137:4685–90.

[12] Wada S, Udagawa N, Nagata N, Martin TJ, Findlay DM. Physiological levels of calcitonin regulate the mouse osteoclast calcitonin receptor by a protein kinase Alpha-mediated mechanism. Endocrinology 1996;137:312–20.

[13] Takahashi S, Goldring S, Katz M, Hilsenbeck S, Williams R, Roodman GD. Downregulation of calcitonin receptor mRNA expression by calcitonin during human osteoclast-like cell differentiation. J Clin Invest 1995;95:167–71.

[14] Kodaira Y. Toxic Substances to Insects, Produced by *Aspergillus ochraceus* and *Oopsra destructor*. Agr Biol Chem 1961;25:261–2.

[15] Ayer WA, Pena-Rodriguez LM. Metabolites produced by alternaria brassicae, the black spot pathogen of canola. Part 1, the phytotoxic components. J Nat Prod 1987;50:400–7.

[16] Akatsu T, Tamura T, Takahashi N, Udagawa N, Tanaka S, Sasaki T, Yamaguchi A, Nagata N, Suda T. Preparation and characterization of a mouse osteoclast-like multinucleated cell population. J Bone Miner Res 1992;7:1297–306.

[17] Takami M, Woo JT, Nagai K. Osteoblastic cells induce fusion and activation of osteoclasts through a mechanism independent of macrophage-colony-stimulating factor production. Cell Tissue Res 1999; 298:327–34.

[18] Bradfisch GA, Harmer SL. omega-Conotoxin GVIA and nifedipine inhibit the depolarizing action of the fungal metabolite, destruxin B on muscle from the tobacco budworm (Heliothis virescens). Toxicon 1990;28:1249–54.

[19] Pedras MS, Zaharia IL, Gai Y, Zhou Y, Ward DE. In planta sequential hydroxylation and glycosylation of a fungal phytotoxin: avoiding cell death and overcoming the fungal invader. Proc Natl Acad Sci USA 2001;98:747–52.

[20] Pedras MS, Biesenthal CJ, Zaharia IL. Comparison of the phytotoxic activity of the phytotoxin destruxin B and four natural analogs. Plant Sci 2000;156:185–92.

[21] Odier F, Vey A, Bureau JP. In vitro effect of fungal cyclodepsipeptides on leukemic cells: study of destruxins A, B and E. Biol Cell 1992;74:267–71.

[22] Morel E, Pais M, Turpin M, Guyot M. Cytotoxicity of cyclodepsipeptides on murine lymphocytes and on L 1210 leukemia cells. Biomed Pharmacother 1983;37:184–5.

[23] Chen HC, Chou CK, Sun CM, Yeh SF. Suppressive effects of destruxin B on hepatitis B virus surface antigen gene expression in human hepatoma cells. Antiviral Res 1997;34:137–44.

[24] Yeh SF, Pan W, Ong GT, Chiou AJ, Chuang CC, Chiou SH, Wu SH. Study of structure-activity correlation in destruxins, a class of cyclodepsipeptides possessing suppressive effect on the generation of hepatitis B virus surface antigen in human hepatoma cells. Biochem Biophys Res Commun 1996;229:65–72.

[25] Sun CM, Chen HC, Yeh SF. Suppressive effects of metabolites from Alternaria brassicaea on the hepatitis B surface antigen. Planta Med 1994;60:87–8.

[26] Nakamura I, Sasaki T, Tanaka S, Takahashi N, Jimi E, Kurokawa T, Kita Y, Ihara S, Suda T, Fukui Y. Phosphatidylinositol-3 kinase is involved in ruffled border formation in osteoclasts. J Cell Physiol 1997;172:230–9.

[27] Nakamura I, Takahashi N, Sasaki T, Tanaka S, Udagawa N, Murakami H, Kimura K, Kabuyama Y, Kurokawa T, Suda T, Fukui Y. Wortmannin, a specific inhibitor of phosphatidylinositol-3 kinase, blocks osteoclastic bone resorption. FEBS Lett 1995;361:79–84.

[28] Woo JT, Kasai S, Stern PH, Nagai K. Compactin suppresses bone resorption by inhibiting the fusion of prefusion osteoclasts and disrupting the actin ring in osteoclasts. J Bone Miner Res 2000;15:650–62.

[29] Zhang D, Udagawa N, Nakamura I, Murakami H, Saito S, Yamasaki K, Shibasaki Y, Morii N, Narumiya S, Takahashi N, Suda T. The small GTP-binding protein, rho p21, is involved in bone resorption by regulating cytoskeletal organization in osteoclasts. J Cell Sci 1995; 108:2285–92.

[30] Chellaiah MA, Soga N, Swanson S, McAllister S, Alvarez U, Wang D, Dowdy SF, Hruska KA. Rho-A is critical for osteoclast podosome organization, motility, and bone resorption. J Biol Chem 2000;275: 11993–2002.

[31] Dumas C, Matha V, Quiot JM, Vey A. Effects of destruxins, cyclic depsipeptide mycotoxins, on calcium balance and phosphorylation of intracellular proteins in lepidopteran cell lines. Comp Biochem Physiol C 1996;114:213–9.

[32] Muroi M, Shiragami N, Takatsuki A. Destruxin B, a specific and readily reversible inhibitor of vacuolar-type H^+-translocat ATPase. Biochem Biophys Res Commun 1994;205:1358–65.

[33] Bandani AR, Amiri B, Butt TM, Gordon-Weeks R. Effects of efrapeptin and destruxin, metabolites of entomogenous fungi, on the hydrolytic activity of a vacuolar type ATPase identified on the brush border membrane vesicles of Galleria mellonella midgut and on plant membrane bound hydrolytic enzymes. Biochim Biophys Acta 2001; 1510:367–77.

[34] Togashi K, Kataoka T, Nagai K. Characterization of a series of vacuolar type H^+-ATPase inhibitors on CTL-mediated cytotoxicity. Immunol Lett 1997;55:139–44.

[35] Naganuma S, Kuzuya N, Sakai K, Hasumi K, Endo A. Inhibition of the accumulation of lipid droplets in macrophage J774 by bafilomycin B1 and destruxin E. Biochim Biophys Acta 1992;1126:41–8.

[36] Cai P, Smith D, Katz B, Pearce C, Venables D, Houck D. Destruxin-A4 chlorohydrin, a novel destruxin from fungus OS-F68576: isolation, structure determination, and biological activity as an inducer of erythropoietin. J Nat Prod 1998;61:290–3.

[37] Tsunoo A, Kamijo M. Non-cyclic AMP-dependent, positive inotropic cyclodepsipeptides with negative chronotropy. J Pharmacol Exp Ther 1999;290:1006–12.

[38] Sato M, Sardana MK, Grasser WA, Garsky VM, Murray JM, Gould RJ. Echistatin is a potent inhibitor of bone resorption in culture. J Cell Biol 1990;111:1713–23.

[39] Dresner-Pollak R. Rosenblatt M. Blockade of osteoclast-mediated bone resorption through occupancy of the integrin receptor: a potential approach to the therapy of osteoporosis. J Cell Biochem 1994; 56:323–30.
[40] Yoneda T, Lowe C, Lee CH, Gutierrez G, Niewolna M, Williams PJ, Izbicka E, Uehara Y, Mundy GR. Herbimycin A, a pp60c-src tyrosine kinase inhibitor, inhibits osteoclastic bone resorption in vitro and hypercalcemia in vivo. J Clin Invest 1993;91:2791–5.
[41] Hall TJ, Schaeublin M, Missbach M. Evidence that c-src is involved in the process of osteoclastic bone resorption. Biochem Biophys Res Commun 1994;199:1237–44.
[42] Razzouk S, Lieberherr M, Cournot G. Rac-GTPase, osteoclast cytoskeleton and bone resorption. Eur J Cell Biol 1999;78:249–55.
[43] Coxon FP, Helfrich MH, Van't Hof R, Sebti S, Ralston SH, Hamilton A, Rogers MJ. Protein geranylgeranylation is required for osteoclast formation, function, and survival: inhibition by bisphosphonates and GGTI-298. J Bone Miner Res 2000;15:1467–76.

0013-7227/03/$15.00/0
Printed in U.S.A.

Endocrinology 144(11):4999–5005

doi: 10.1210/en.2003-0166

p38 Mitogen-Activated Protein Kinase Is Crucially Involved in Osteoclast Differentiation But Not in Cytokine Production, Phagocytosis, or Dendritic Cell Differentiation of Bone Marrow Macrophages

XIAOTONG LI, NOBUYUKI UDAGAWA, MASAMICHI TAKAMI, NOBUAKI SATO, YASUHIRO KOBAYASHI, AND NAOYUKI TAKAHASHI

Institute for Oral Science (X.L., Y.K., N.T.), Department of Biochemistry (N.U., N.S.), Matsumoto Dental University, Nagano 399-0781, Japan; Department of Biochemistry (M.T.), School of Dentistry, Showa University, Tokyo 142-8555, Japan; and Department of Periodontology (N.S.), School of Dentistry, Aichi Gakuin University, Aichi 464-8651, Japan

We previously reported that p38 MAPK signaling is required for osteoclast differentiation but not osteoclast function. Here we further investigated the role of p38 MAPK in the function and differentiation of mouse bone marrow macrophages (BMMϕ), common precursors of osteoclasts and dendritic cells. Lipopolysaccharide (LPS) activated the p38 MAPK signaling pathway in BMMϕ by sequential phosphorylation of MAPK kinase 3/6, p38 MAPK, and activating transcription factor-2. Treatment of BMMϕ with SB203580, a p38 MAPK inhibitor, suppressed LPS-induced phosphorylation of activating transcription factor-2. LPS stimulated production of IL-1β, TNFα, and IL-6 in BMMϕ, and SB203580 failed to inhibit the LPS-induced cytokine production. BMMϕ incorporated latex beads via phagocytosis, and SB203580 had no effect on this phagocytosis. BMMϕ differentiated into dendritic cells when treated with granulocyte macrophage colony-stimulating factor together with CD40 ligand, TNFα, or LPS, and SB203580 failed to inhibit this differentiation. Thus, p38 MAPK-mediated signals are not involved in either BMMϕ function or BMMϕ differentiation into dendritic cells. The differentiation of BMMϕ into osteoclasts in response to receptor activator of nuclear factor-κB ligand or TNFα was strongly inhibited by SB203580. These findings emphasize the crucial roles of p38 MAPK-mediated signaling in osteoclast differentiation. (*Endocrinology* 144: 4999–5005, 2003)

HEMOPOIETIC CELLS OF the monocyte-macrophage lineage differentiate into bone-resorbing osteoclasts under the control of osteoblasts or bone marrow stromal cells (1–4). Osteoblasts/stromal cells express two factors essential for osteoclastogenesis, RANKL [receptor activator of nuclear factor-κB (RANK) ligand] and macrophage colony-stimulating factor (M-CSF) (1–4). RANKL together with M-CSF induces osteoclast formation from monocytes/macrophages in the absence of osteoblasts/stromal cells. Mature osteoclasts as well as osteoclast precursors express RANK, a receptor of RANKL, and RANKL stimulates the survival, fusion and bone-resorbing activity of osteoclasts. TNFα has been shown to stimulate osteoclast differentiation from monocytes/macrophages through a mechanism independent of RANKL-RANK interaction (5, 6).

Monocytes/macrophages play critical roles in innate defenses against viral and bacterial infections. They produce proinflammatory cytokines such as IL-1β, TNFα, and IL-6 in response to viral and bacterial constituents (7–9). These cytokines activate the immune system to defend the host from infections. Another important function by which macrophages fight infectious diseases is phagocytosis (10). Macrophages show strong phagocytic activity against foreign substances. In addition, monocyte/macrophage-lineage cells can give rise not only to osteoclasts but also to dendritic cells, antigen-presenting immune cells (11–13). Monocyte/macrophage lineage cells differentiate into immature dendritic cells in the presence of granulocyte macrophage colony-stimulating factor (GM-CSF) (14, 15). CD40 ligand (CD40L), TNFα, or lipopolysaccharide (LPS) then stimulates the maturation of GM-CSF-induced immature dendritic cells (16).

The p38 MAPK family is a group of 38-kDa intracellular signal transduction proteins (17–19). c-Jun N-terminal kinase and ERK, together with p38 MAPK, form the MAPK family (19). p38 MAPK is predominantly activated through its phosphorylation by upstream MAPK kinase 3 (MKK3) and MKK6 (17, 18). Activated p38 MAPK then phosphorylates downstream targets, including activating transcription factor-2 (ATF-2). SB203580, a specific inhibitor of p38 MAPK, has been widely used to investigate the roles of p38 MAPK in the differentiation and function of cells (17–19). SB203580 binds to the ATP pocket of the activated p38 MAPK and inhibits phosphorylation of the downstream targets (19). Recent studies have shown that signals mediated by p38 MAPK are involved in the differentiation of chondrocytes and epithelial cells (20, 21). Kumar *et al.* (22) also reported that SB203580 inhibited IL-6 production induced by IL-1 and TNFα in osteoblasts and chondrocytes. These results suggest that p38 MAPK-mediated signals are involved in cell differentiation and function.

Abbreviations: ATF2, Activating transcription factor-2; BMMϕ, bone marrow macrophages; CD40L, CD40 ligand; FBS, fetal bovine serum; GAPDH, glyceraldehyde-3-phosphate dehydrogenase; GM-CSF, granulocyte macrophage colony-stimulating factor; LPS, lipopolysaccharide; M-CSF, macrophage colony-stimulating factor; MKK, MAPK kinase; RANK, receptor activator of nuclear factor-κB ligand; RANKL, RANK ligand; TRAP, tartrate-resistant acid phosphatase.

We and others (23, 24) have reported that SB203580 inhibits RANKL-induced differentiation of precursor cells into osteoclasts, Interestingly, it was previously found that SB203580 fails to inhibit the survival and bone-resorption activity of osteoclasts induced by RANKL. Moreover, p38 MAPK is phosphorylated in response to RANKL, IL-1, TNFα, and LPS in bone marrow macrophages (BMMϕ), which are the osteoclast precursors, but not in mature osteoclasts (23). We therefore concluded that p38 MAPK-mediated signals are required for osteoclast differentiation but not osteoclast function. It was also shown that RANKL is a survival factor of dendritic cells (25).

In the present study, we further investigated the role of p38 MAPK-mediated signaling in the function and differentiation of BMMϕ, common precursors of osteoclasts and dendritic cells. We showed here that inhibition of p38 MAPK activity by SB203580 in BMMϕ did not suppress the cytokine production or phagocytic activity of BMMϕ. SB203580 failed to inhibit dendritic cell differentiation of BMMϕ, whereas it strongly inhibited the induction of BMMϕ differentiation into osteoclasts by RANKL and TNFα. These findings suggest that p38 MAPK-mediated signaling is crucially involved in osteoclast differentiation.

Materials and Methods

Animals and chemicals

Five- to 8-wk-old male ddY mice were obtained from Shizuoka Laboratories Animal Center (Shizuoka, Japan). Three- to 4-wk-old C57BL/6J mice were obtained from The Jackson Laboratory (Bar Harbor, ME). All procedures for animal care were approved by the Animal Management Committee of Matsumoto Dental University. Recombinant human M-CSF (Leukoprol) was obtained from Kyowa Hakko Kogyo Co. (Tokyo, Japan). Recombinant murine GM-CSF and soluble RANKL were purchased from PeproTech EC Ltd. (London, UK). Mouse TNFα was obtained from Genzyme TECHNE (Minneapolis, MN). Mouse CD8-conjugated CD40L in insect cell culture supernatant was provided by Dr. Yongwon Choi (University of Pennsylvania, Philadelphia, PA). LPS was purified from *Escherichia coli* strain K235 as described (26). SB203580 was purchased from Calbiochem Co. (La Jolla, CA). Latex beads (0.75-μm microspheres, 2.68%) were from Polysciences, Inc. (Warrington, PA). Rabbit polyclonal antibodies against phospho-p38 MAPK, p38 MAPK, phospho-MKK3/6, MKK3, phospho-ATF-2, ATF-2, phospho-ERK, and ERK were purchased from Cell Signaling Technology, Inc. (Beverly, MA). ELISA kits for mouse IL-1β and TNFα were obtained from Genzyme TECHNE, and that for mouse IL-6 was obtained from ENDOGEN (Woburn, MA). Specific PCR primers for mouse IL-1β, IL-6, TNFα, and glyceraldehyde-3-phosphate dehydrogenase (GAPDH) were synthesized by Life Technologies, Inc. (Tokyo, Japan). Other chemicals and reagents were of analytical grade.

Preparation of mouse bone marrow macrophages

Bone marrow cells obtained from tibiae of 5- to 8-wk-old adult mice were suspended in αMEM (Sigma, St. Louis, MO) supplemented with 10% fetal bovine serum (FBS) (JRH Biosciences, Lenexa, KS) in 60-mm diameter dishes for 16 h in the presence of M-CSF (100 ng/ml) (5). Then, nonadherent cells were harvested and further cultured for 2 d with M-CSF (100 ng/ml). Nonadherent cells were completely removed from the cultures by pipetting. The adherent cells, almost all of which expressed macrophage-specific antigens such as Mac-1, Moma-2, and F4/80, were used as BMMϕ (5). Usually, bone marrow cells from three animals were pooled and used for the BMMϕ preparation in each experiment.

Osteoclast differentiation

BMMϕ were further cultured for 4 d with M-CSF (100 ng/ml) together with RANKL (100 ng/ml) or TNFα (20 ng/ml) in 48-well plates in the presence or absence of SB203580 at 10^{-7} M or 10^{-6} M. Cells were then fixed and stained for tartrate-resistant acid phosphatase (TRAP; a marker enzyme of osteoclasts) as described (27). TRAP-positive multinucleated cells judged by microscopic examination contain three or more nuclei were counted as osteoclasts. The number of osteoclasts formed in the culture varied greatly in each experiment (28). Therefore, the results obtained from one experiment typical of three independent experiments were expressed as the means ± SD of three cultures. The significance of the differences was determined using Student's *t* test.

Cytokine production and phagocytosis assay

BMMϕ were further cultured for 48 h with vehicle (control) or LPS (1 μg/ml). Some cultures were pretreated with SB203580 (10^{-6} M) overnight in the presence of M-CSF (100 ng/ml). The concentrations of IL-1β, TNFα, and IL-6 in the conditioned medium were determined using the respective ELISA kits. BMMϕ were cultured on 18-mm coverslips in 12-well plates at 10^5 cells/1 ml/well with M-CSF (100 ng/ml) in the presence or absence of SB203580 at 10^{-6} M. BMMϕ were further maintained in serum-free αMEM for 4 h, and then latex beads (1:500 dilution) were added to each well for 10 min, 20 min, 40 min, or 1 h. The cells on the coverslips were then rinsed twice with cold PBS, fixed with methanol and stained with Giemsa's solution. Cells containing latex beads were counted as bead-positive cells. Phagocytic activity of macrophages was measured as the percentage of bead-positive cells among the total cells. The results obtained from one typical experiment of three independent experiments were expressed as the means ± SD of three cultures.

Dendritic cell differentiation

Bone marrow cells prepared from C57BL/6J mice were suspended in αMEM supplemented with 10% FBS in 100-mm diameter dishes (10^7 cells/10 ml/dish) in the presence of M-CSF (30 ng/ml). After the cells were cultured for 2 d, the adherent cells were harvested by treatment with 0.05% trypsin and EDTA (Life Technologies, Inc.) for 5 min. The harvested cells were resuspended in RPMI 1640 medium (Sigma) supplemented with 5% FBS, because dendritic cell differentiation from BMMϕ is generally examined in this culture condition (29). At d 0, cells were seeded in 24-well plates (2×10^5 cells/0.5 ml/well) with GM-CSF (10 ng/ml) in the presence of increasing concentrations of SB203580. On d 2, two thirds of the culture supernatant was replaced with fresh medium containing the same concentrations of GM-CSF and SB203580. On d 4, another milliliter of fresh medium containing CD40L (1:500 dilution of the original solution), TNFα (20 ng/ml final concentration) or LPS (1 μg/ml final concentration) was added to some cultures to stimulate the maturation of dendritic cells. After further culturing for 2 d, the cells were stained with biotin-conjugated anti-CD11c antibody followed by streptavidin-fluorescein isothiocyanate and phycoerythrin-conjugated CD86 antibody (all from BD PharMingen, San Diego, CA). The stained cells were analyzed by fluorescence-activated cell sorting as described (29).

PCR amplification of reverse-transcribed mRNA

BMMϕ were cultured for 24 h in αMEM containing 10% FBS with vehicle (control) or LPS (1 μg/ml) in the presence or absence of SB203580 (10^{-6} M) on 60-mm diameter dishes. Some cultures of BMMϕ were pretreated with SB203580 (10^{-6} M) for overnight in the presence of M-CSF (100 ng/ml). Total cellular RNA was then extracted using TRIzol solution (Life Technologies, Inc.). First-strand cDNA was synthesized from total RNA with random primers and subjected to PCR amplification with Ex *Taq* polymerase (Takara Biochemicals, Shiga, Japan) using the following specific PCR primers: mouse IL-1β, 5′-AAGCTCTCCACCTCAATGGA-3′ (forward, nucleotides 431–450) and 5′-TGCTTGAGAGGTGCTGATGT-3′ (reverse, nucleotides 713–732); mouse TNFα, 5′-ACGTGGAACTGGCAGAAGAG-3′ (forward, nucleotides 26–45) and 5′-TGGAAGACTCCTCCCAGGTA-3′ (reverse, nucleotides 589–608); mouse IL-6, 5′-TTCCATCCAGTTGCCTTCTT-3′ (forward, nucleotides 26–45) and 5′-TCTTGGTCCTTAGCCACTCC-3′ (reverse,

nucleotides 546–565); and mouse GAPDH, 5′-ACCACAGTCCATGCCATCAC-3′ (forward, nucleotides 566–585) and 5′-TCCACCACCCTGTTGCTGTA-3′ (reverse, nucleotides 998–1017). The PCR products were separated by electrophoresis on 2% agarose gels and visualized by ethidium bromide staining with UV light illumination. The sizes of the PCR products for mouse IL-1β, TNFα, IL-6, and GAPDH were 302, 583, 541, and 452 bp, respectively.

Western blot analysis

BMMϕ prepared in 60-mm diameter dishes were further incubated with vehicle (control), or LPS (1 μg/ml) in the presence or absence of SB203580 (10^{-6} M) for 30 min, and then washed twice with PBS and lysed in cell lysate buffer [62.5 mM Tris-HCl (pH 6.8), 2% sodium dodecyl sulfate, 10.2% 2-mercaptoethanol, 10% glycerol, and 0.01% bromophenol blue]. Some cultures of BMMϕ were pretreated with SB203580 (10^{-6} M) overnight in the presence of M-CSF (100 ng/ml). Whole cell extracts were electrophoresed on a 10% SDS-polyacrylamide gel and transferred onto a nitrocellulose membrane (Millipore, Bedford, MA). After blocking with 5% skim milk in Tris-buffered saline containing 0.1% Tween 20 (TBS-T), the anti-phospho-MKK3/6 antibody, anti-MKK3 antibody, anti-phospho-p38 MAPK antibody, anti-p38 MAPK antibody, anti-phospho-ATF2 antibody, anti-ATF2 antibody, anti-phospho-ERK antibody or anti-ERK antibody (1:1000 dilution) was added in TBS-T containing 5% BSA, and the bound antibodies were visualized by using the enhanced chemiluminescence (ECL) assay with reagents from Amersham Co. (Arlington Heights, IL) followed by exposure to x-ray film.

TABLE 1. Effect of SB203580 on CD40L-induced dendritic cell maturation[a]

SB203580 (M)	Mature dendritic cells (%)	
	Control	CD40L
0	17.8 ± 2.3	80.7 ± 2.2
10^{-7}	17.4 ± 1.1	80.8 ± 1.6
10^{-6}	16.4 ± 2.6	79.2 ± 3.9

[a] Bone marrow cell-derived dendritic cells were prepared with or without CD40L (1:1000 dilution of the original solution) in the presence or absence of SB203580 at the indicated concentrations. Cells were stained with antibodies for CD11c and CD86 and analyzed by FACS. The results are expressed as the means ± SD of three independent experiments.

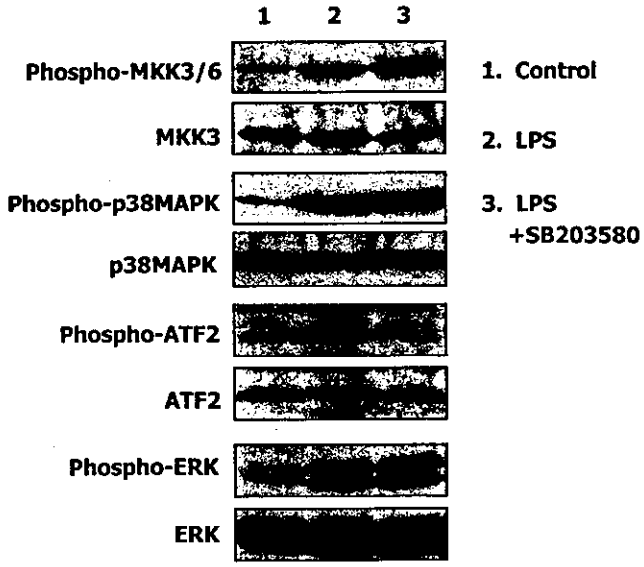

FIG. 1. Effect of SB203580 on the phosphorylation of MKK3/6, p38 MAPK, ATF2, and ERK induced by LPS in BMMϕ. Bone marrow cells were cultured for 16 h with M-CSF (100 ng/ml) as described in *Materials and Methods*. Then nonadherent cells were harvested and further cultured with M-CSF (100 ng/ml). After culturing for 2 d, nonadherent cells were carefully removed, and adherent cells were used as BMMϕ. Some cultures of BMMϕ were pretreated with SB203580 (10^{-6} M) overnight in the presence of M-CSF (100 ng/ml). BMMϕ were then incubated with LPS (1 μg/ml) for 30 min in the presence or absence of SB203580 (10^{-6} M), and total-cell lysates were prepared. The lysates were separated by SDS-PAGE, transferred onto nitrocellulose membranes, and immunoblotted with the indicated antibodies (1:1000 dilution).

Results

BMMϕ were prepared from mouse bone marrow cultures treated with M-CSF for 3 d. When BMMϕ were treated with RANKL and M-CSF, more than 70% of BMMϕ differentiated into TRAP-positive mononuclear cells and multinucleated cells within 4 d. SB203580, a specific inhibitor of p38 MAPK, strongly inhibited the induction of osteoclast differentiation by RANKL (see Table 1). We first examined whether SB203580 specifically blocked p38 MAPK signaling in BMMϕ (Fig. 1). SB203580 is known to bind to the ATP binding site of the activated p38 MAPK and to inhibit the kinase activity (19). We found that MKK3/6, p38 MAPK, ATF2, and ERK were markedly phosphorylated in BMMϕ treated with LPS for 30 min. We previously showed that RANKL and TNFα

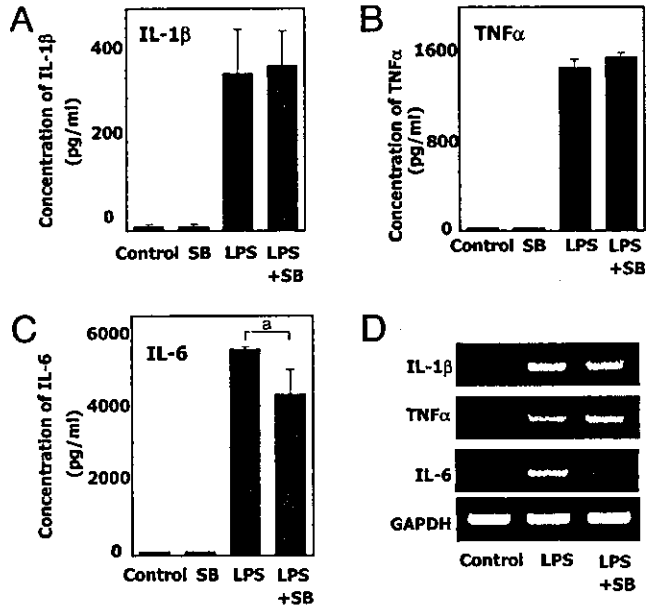

FIG. 2. Effect of SB203580 on the production of IL-1β, TNFα, and IL-6 induced by LPS in mouse BMMϕ. BMMϕ were prepared in 48-well plates. Some cultures of BMMϕ were pretreated with SB203580 (10^{-6} M) overnight. The BMMϕ were then incubated with or without LPS (1 μg/ml) for 48 h in the presence or absence of SB203580 (10^{-6} M). The conditioned medium of each well was collected and the concentrations of IL-1β (A), TNFα (B), and IL-6 (C) in the conditioned medium were measured using the respective ELISA kits. The results were expressed as the means ± SD of three cultures. D, BMMϕ were prepared in 60 mm diameter dishes. Some cultures of BMMϕ were also pretreated with SB203580 (10^{-6} M) for overnight. The BMMϕ were then incubated for 24 h with LPS (1 μg/ml) in the presence or absence of SB203580 (10^{-6} M). Total RNA was then extracted from BMMϕ, and the expression of IL-1β, TNFα, IL-6, and GAPDH mRNAs was analyzed by RT-PCR. The PCR products for IL-1β, TNFα, IL-6, and GAPDH were 302, 583, 541, and 452 bp, respectively. [a], Significantly different from the culture treated with LPS; $P < 0.05$.

as well as LPS stimulate phosphorylation of p38 MAPK in BMMϕ (24). SB203580 did not inhibit LPS-induced phosphorylation of p38 MAPK, ERK, or MKK3/6, which is the upstream activator of p38 MAPK, but strongly suppressed the phosphorylation of ATF2, which is one of the downstream targets of p38 MAPK (Fig. 1). The total amounts of the MKK3, p38 MAPK, ERK, and ATF2 proteins in BMMϕ remained unchanged in the presence and absence of LPS and/or SB203580 (Fig. 1). Altogether, these results demonstrate that SB203580 inhibited p38 MAPK-mediated signaling in BMMϕ.

The role of p38 MAPK-mediated signaling in BMMϕ function was then examined using SB203580. Treatment of BMMϕ with LPS for 48 h markedly stimulated the production of proinflammatory cytokines such as IL-1β, TNFα, and IL-6 in BMMϕ (Fig. 2, A–C). BMMϕ were preincubated with SB203580 overnight and further treated with LPS together with SB203580. The SB compound showed no inhibitory effect on the LPS-induced production of IL-1β and TNFα in BMMϕ (Fig. 2, A and B). RT-PCR analysis confirmed that the expression of IL-1β and TNFα mRNAs in BMMϕ was upregulated by LPS, and SB203580 showed no inhibitory effects on the mRNA expression (Fig. 2D). There was a downward trend in IL-6 production in the presence of SB203580 at both the mRNA and protein levels, but the inhibitory effect of SB203580 was not marked (Fig. 2, C and D). These results suggest that p38 MAPK activity is not crucially involved in the production of these cytokines in BMMϕ.

Macrophages can ingest great quantities of latex beads by phagocytosis. We next examined whether phagocytosis of BMMϕ is affected by the treatment of BMMϕ with SB203580. BMMϕ were incubated with latex beads for 10–60 min, and the BMMϕ that incorporated latex beads were counted as phagocytic cells (Fig. 3A). The number of BMMϕ incorporating latex leads increased as the incubation period increased. Almost all BMMϕ showed phagocytic activity within 60 min (Fig. 3A). The time course of changes in the phagocytosis of BMMϕ was not affected by the addition of SB203580. The phagocytic activity of BMMϕ was also evaluated after incubation for 40 min. The proportions of BMMϕ incorporating more than 100 latex beads, 50–100 beads, and less than 50 beads were about 10%, 25%, and 50% of total BMMϕ, respectively (Fig. 3, B and C). Again, SB203580 failed to inhibit the phagocytic activity of BMMϕ.

Finally, we examined the possible involvement of p38 MAPK-mediated signaling in dendritic cell differentiation, because dendritic cells differentiate from the same precursors as osteoclasts. BMMϕ were cultured for 4 d in the presence of GM-CSF to induce dendritic cell differentiation. The cells were further cultured for 2 d in the presence of GM-CSF with or without CD40L to induce their maturation (Fig. 4A). Without CD40L stimulation, the majority of the cells were

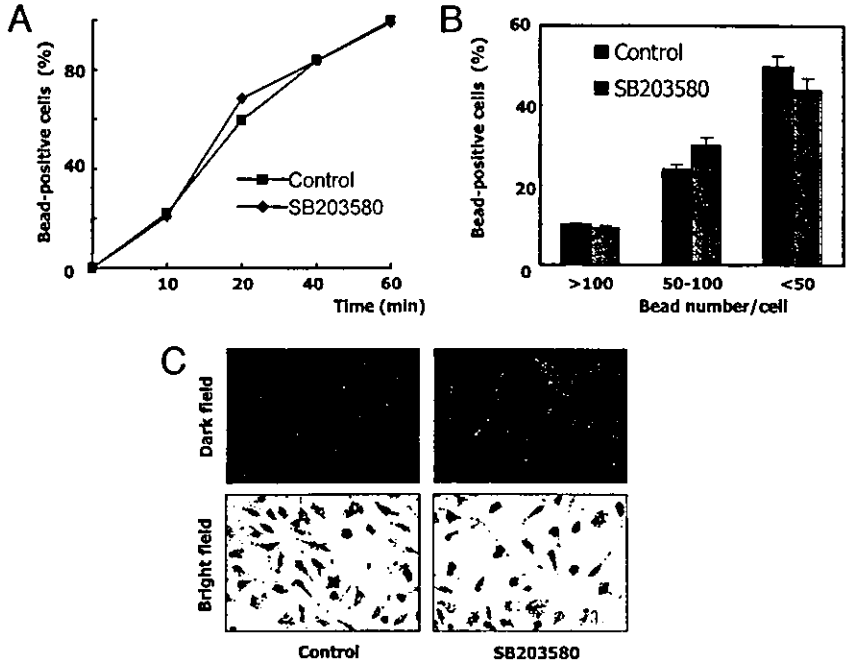

FIG. 3. Effect of SB203580 on the phagocytosis of BMMϕ. BMMϕ were prepared on 18-mm diameter glass coverslips in 12-well plates. BMMϕ were then maintained in serum-free medium for 4 h. Some cultures of BMMϕ were preincubated with SB203580 (10^{-6} M) for overnight, and maintained in serum-free medium in the presence of SB203580. BMMϕ were incubated with latex beads for 10 min, 20 min, 40 min, or 1 h in the presence or absence of SB203580 (10^{-6} M). BMMϕ on coverslips were then fixed and stained with Giemsa's solution, and observed by microscopic examination. A, Time course of changes of phagocytic activity in BMMϕ treated or not treated with SB203580. Cells incorporating beads were counted as bead-positive cells. The percentage of bead-positive cells was calculated at the indicated time points. The SD was small enough to be included at each mean point. B, Effect of SB203580 on phagocytic activity of BMMϕ. BMMϕ were incubated with latex beads for 40 min. Cells incorporating beads were counted as bead-positive cells, and divided into three groups according to the number of beads incorporated (>100 beads, 50–100 beads, <50 beads) in each cell. The percentage of bead-positive cells was calculated. C, Dark- and bright-field images of BMMϕ treated or not treated with SB203580. BMMϕ were incubated with latex beads for 40 min. Latex beads incorporated in BMMϕ appeared as *bright green dots* in the dark field with UV light illumination (*upper panels*). Nuclei of BMMϕ appeared in *purple* in the bright field (*lower panels*). *Bar*, 50 μm.

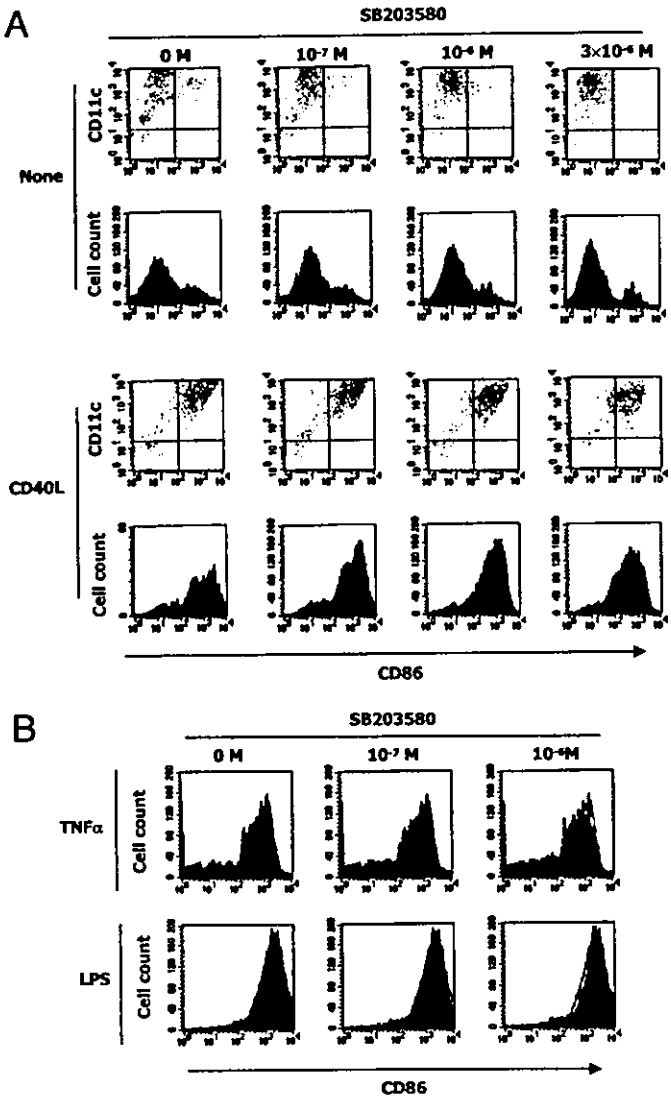

FIG. 4. Effect of SB203580 on the differentiation and maturation of dendritic cells. BMMϕ were cultured for 4 d in 24-well plates (2×10^5 cells/1 ml/well) with GM-CSF (10 ng/ml) to induce the dendritic cell differentiation in the presence of SB203580 at the indicated doses. Then, the culture was further treated for 2 d with or without CD40L (1:1000 dilution of the original solution), TNFα (20 ng/ml) or LPS (1 μg/ml) to stimulate the maturation of dendritic cells in the presence or absence of SB203580. Cells were stained with antibodies for CD11c and CD86, and analyzed by fluorescence-activated cell sorting. Dot plots show the expression of CD11c and CD86 on the cells (*upper panels* in A). Histograms show the distribution of CD86-positive cells in the CD11c-positive cell population (*lower panels* in A and B).

CD11c (a marker of dendritic cells) positive and CD86 (a marker of mature dendritic cells) negative (Fig. 4A, *upper panels*). With CD40L stimulation, the majority of the cells were CD11c and CD86 double positive (Fig. 4A, *lower panels*). SB203580 at 10^{-7} M to 3×10^{-6} M had no effect on the expression of either CD11c or CD86 (Fig. 4A, *upper panels*). Treatment with TNFα or LPS similarly stimulated the maturation of dendritic cells in the presence of GM-CSF (Fig. 4B). The induction of dendritic cell maturation by TNFα and LPS was not affected by the addition of SB203580 (Fig. 4B).

The effect of SB203580 on CD40L-induced dendritic cell differentiation was compared with that on RANKL- and TNFα-induced osteoclast differentiation. CD40L markedly increased the number of CD86-positive mature dendritic cells (Table 1). The induction of dendritic cell maturation by CD40L was not affected by SB203580 even at 10^{-6} M. Treatment of BMMϕ with RANKL or TNFα stimulated osteoclast formation (Table 2). SB203580, even at 10^{-7} M, inhibited the induction of osteoclastic differentiation of BMMϕ by RANKL (33.4 ± 15.4% of the control, the mean ± SD of experiments 1–3) and TNFα (45.6 ± 11.7% of the control, the mean ± SD of experiments 4–6). SB203580 at 10^{-7} M showed no inhibitory effect on the dendritic cell differentiation induced by CD40L, TNFα or LPS (Fig. 4). Neither cytokine production nor phagocytic activity of BMMϕ was significantly inhibited by 10^{-7} M SB2035807 (data not shown).

TABLE 2. Effect of SB203580 on RANKL- and TNFα-induced osteoclast differentiation[a]

SB203580 (M)	Osteoclasts (cells/well)	
	RANKL	TNFα
	Experiment 1	Experiment 4
0	536.5 ± 6.6	70.0 ± 5.0
10^{-7}	111.0 ± 9.2[e]	25.3 ± 8.1[d]
10^{-6}	80.0 ± 11.2[e]	12.0 ± 2.6[e]
	Experiment 2	Experiment 5
0	116.0 ± 16.5	73.7 ± 13.2
10^{-7}	58.7 ± 17.4[d]	31.0 ± 1.7[c]
10^{-6}	9.0 ± 5.3[e]	9.7 ± 5.7[d]
	Experiment 3	Experiment 6
0	152.0 ± 16.1	43.0 ± 7.9
10^{-7}	43.7 ± 12.6[e]	25.3 ± 8.1
10^{-6}	23.0 ± 5.6[e]	21.0 ± 2.6[b]

[a] BMMϕ were cultured for 4 d with M-CSF (100 ng/ml) together with RANKL (100 ng/ml) or TNFα (20 ng/ml) in 48-well plates in the presence or absence of SB203580 at the indicated concentrations. TRAP-positive multinucleated cells containing three or more nuclei were counted as osteoclasts. No TRAP-positive osteoclasts were formed in the absence of RANKL or TNFα. The results were expressed as the means ± SD of three cultures.

[b,c,d,e] Significantly different from the culture treated without SB203580; [b] $P < 0.05$, [c] $P < 0.01$, [d] $P < 0.005$, [e] $P < 0.001$.

Discussion

Using SB203580, a specific inhibitor of p38 MAPK, we investigated the roles of p38 MAPK in the function and differentiation of BMMϕ, the common precursors of osteoclasts and dendritic cells. Pretreatment of BMMϕ with SB203580 inhibited the induction of ATF2 phosphorylation by LPS, suggesting that SB203580 shuts off the p38 MAPK-mediated signaling in BMMϕ. However, SB203580 failed to inhibit LPS-induced production of IL-1β and TNFα by BMMϕ. LPS-induced IL-6 production in BMMϕ was only slightly inhibited by SB203580. Moreover, SB203580 had no inhibitory effect on the phagocytic activity of BMMϕ. BMMϕ differentiated into dendritic cells in the presence of GM-CSF, and matured in response to the stimulation by CD40L, TNFα or LPS. SB203580 again failed to inhibit the differentiation and maturation of dendritic cells. In the present study, dendritic cell differentiation was examined in cultures of BMMϕ derived from C57BL/6J mice, whereas osteoclast differentiation was examined in cultures of BMMϕ from ddY mice. We have confirmed that BMMϕ derived from C57BL/6J mice

differentiated similarly into osteoclasts in response to RANKL or TNFα, and the osteoclast differentiation was strongly inhibited by SB203580. These results suggest that p38 MAPK-mediated signaling is not involved in either BMMϕ functions such as cytokine production and phagocytosis or dendritic cell differentiation from the common precursors of osteoclasts and dendritic cells.

The role of p38 MAPK in cytokine production and cell differentiation is highly controversial. Baldassare *et al.* (30) reported that SB203580 inhibited the induction of IL-1β production by LPS in RAW264.7 cells and J774 cells, but SB203580 did not alter IL-1β mRNA levels in another ANA-1 macrophage cell line. Rawadi *et al.* (31) showed that Raw 264.7 cells produced IL-1β, TNFα, and IL-6 in response to *Mycoplasma fermentans* membrane lipoproteins, and this production was strongly inhibited by SB203580. In contrast, peritoneal macrophages obtained from MKK3-deficient mice, in which p38 MAPK activation was diminished, produced TNFα normally in response to LPS (32). Yosimichi *et al.* (20) reported that connective tissue growth factor stimulated both differentiation and proliferation of chondrocytes, and the differentiation of chondrocytes induced by connective tissue growth factor was selectively inhibited by SB203580. Bhowick *et al.* (21) also reported that TGFβ induced epithelial to mesenchymal transdifferentiation in mammary epithelial cells, and inhibition of p38 MAPK activity by the expression of a dominant-negative p38 MAPK blocked epithelial to mesenchymal transdifferentiation induced by TGFβ. In contrast, SB203580 has been shown to enhance monocytic differentiation of HL60 cells induced by 1,25-dihydroxyvitamin D_3 (33). These results suggest that the role of p38 MAPK differs in different types of cells and/or different physiological states. The divergence in the effects of SB203580 on several cell types may be due to differences in isoforms of p38 MAPK involved in the differentiation of each cell type. SB203580 has been shown to inhibit p38 MAPK, p38α, and p38β2, but not p38γ (34, 35). It is also possible that the role of p38 MAPK may differ in cells of different origin and/or different states. In some cells, the target of p38 MAPK will function at the translational level (36, 37), whereas in others, its target will function at the transcriptional level (19, 30). Further studies will be necessary to elucidate the different roles of p38 MAPK in cytokine production and cell differentiation.

CD40-mediated signals have been shown to be quite similar to those of RANK (38). Nevertheless, CD40L-induced maturation of dendritic cells was not suppressed by the addition of SB203580. Like RANKL, TNFα has been shown to stimulate osteoclast differentiation from monocyte/macrophage lineage cells, including BMMϕ (5, 6). TNFα-induced osteoclast formation in BMMϕ was strongly inhibited by SB203580 even at 10^{-7} M. Matsumoto *et al.* (23) also reported that treatment of RAW264.7 cells with SB203580 inhibited TNFα-induced osteoclast differentiation. Thus, the p38 MAPK pathway plays a crucial role in not only RANKL-mediated but also TNFα-mediated osteoclast differentiation. In contrast to its effect on osteoclast differentiation, SB203580 failed to inhibit the induction of dendritic cell differentiation and maturation by TNFα as well as CD40L. The induction of human osteoclast formation by RANKL plus M-CSF from CD14-positive cells in peripheral blood was also inhibited by the addition of SB203580 (data not shown). These results emphasize the importance of p38 MAPK-mediated signaling in the differentiation of osteoclasts but not dendritic cells from their common precursors. Recently, a transcription factor, NFAT2 (NFATc1), has been shown to play a critical role in the differentiation of osteoclasts induced by RANKL (39, 40). Therefore, it is proposed that the p38 MAPK signaling is involved in the induction of NFAT2 activation.

We previously reported that osteoclasts expressed a certain amount of p38 MAPK but failed to phosphorylate p38 MAPK in response to any of the stimuli examined (24). LPS did not induce the phosphorylation of MKK3/6 or ATF2 in osteoclasts, suggesting that the p38 MAPK signaling pathway is not entirely functional in osteoclasts. These findings raise novel questions concerning the role of p38 MAPK in osteoclast differentiation and function: why is p38 MAPK-mediated signaling important for osteoclast but not dendritic cell differentiation? How is the p38 MAPK signaling pathway selectively shut down in osteoclasts after the completion of their differentiation? Further studies on p38 MAPK-mediated events in osteoclast precursors will provide new insights into the regulatory mechanisms of osteoclast differentiation and function.

Acknowledgments

Received February 3, 2003. Accepted July 18, 2003.

Address all correspondence and requests for reprints to: Naoyuki Takahashi, Ph.D., Institute for Oral Science, Matsumoto Dental University, 1780 Gobara, Hiro-oka, Shiojiri, Nagano 399-0781, Japan. E-mail: takahashinao@po.mdu.ac.jp.

This work was supported in part by Grants-in-Aid 12137209, 13557155, and 13470394 and a Grant for Asian Researchers awarded by the Tokyo Biochemical Research Foundation, Japan.

References

1. **Suda T, Takahashi N, Udagawa N, Jimi E, Gillespie MT, Martin TJ** 1999 Modulation of osteoclast differentiation and function by the new members of the tumor necrosis factor receptor and ligand families. Endocr Rev 20:345–357
2. **Roodman GD** 1999 Cell biology of the osteoclast. Exp Hematol 27:1229–1241
3. **Teitelbaum SL** 2000 Bone resorption by osteoclasts. Science 289:1504–1508
4. **Chambers TJ** 2000 Regulation of the differentiation and function of osteoclasts. J Pathol 192:4–13
5. **Kobayashi K, Takahashi N, Jimi E, Udagawa N, Takami M, Kotake S, Nakagawa N, Kinosaki M, Yamaguchi K, Shima N, Yasuda H, Morinaga T, Higashio K, Martin TJ, Suda T** 2000 Tumor necrosis factor α stimulates osteoclast differentiation by a mechanism independent of the ODF/RANKL-RANK interaction. J Exp Med 191:275–286
6. **Azuma Y, Kaji K, Katogi R, Takeshita S, Kudo A** 2000 Tumor necrosis factor-α induces differentiation of and bone resorption by osteoclasts. J Biol Chem 275:4858–4864
7. **Lynn WA, Golenbock DT** 1992 Lipopolysaccharide antagonists. Immunol Today 13:271–276
8. **Ulevitch RJ, Tobias PS** 1995 Receptor-dependent mechanisms of cell stimulation by bacterial endotoxin. Annu Rev Immunol 13:437–457
9. **Hla T, Lee MJ, Ancellin N, Paik JH, Kluk MJ** 2001 Lysophospholipids-receptor revelations. Science 294:1875–1878
10. **Djaldetti M, Salman H, Bergman M, Djaldetti R, Bessler H** 2002 Phagocytosis—the mighty weapon of the silent warriors. Microsc Res Tech 57:421–431
11. **Heath WR, Carbone FR** 2001 Cross-presentation, dendritic cells, tolerance and immunity. Annu Rev Immunol 19:47–64
12. **Banchereau J, Steinman RM** 1998 Dendritic cells and the control of immunity. Nature 392:245–252
13. **Flores-Romo L, Bjorck P, Duvert V, van Kooten C, Saeland S, Banchereau J** 1997 CD40 ligation on human cord blood CD34+ hematopoietic progenitors induces their proliferation and differentiation into functional dendritic cells. J Exp Med 185:341–349
14. **Caux C, Vanbervliet B, Massacrier C, Dezutter-Dambuyant C, de Saint-Vis B, Jacquet C, Yoneda K, Imamura S, Schmitt D, Banchereau J** 1996 $CD34^+$

hematopoietic progenitors from human cord blood differentiate along two independent dendritic cell pathways in response to GM-CSF+TNFα. J Exp Med 184:695–706
15. **Young JW, Szabolcs P, Moore MA** 1995 Identification of dendritic cell colony-forming units among normal human $CD34^+$ bone marrow progenitors that are expanded by c-kit-ligand and yield pure dendritic cell colonies in the presence of granulocyte/macrophage colony-stimulating factor and tumor necrosis factor α. J Exp Med 182:1111–1119
16. **Bleharski JR, Niazi KR, Sieling PA, Cheng G, Modlin RL** 2001 Signaling lymphocytic activation molecule is expressed on CD40 ligand-activated dendritic cells and directly augments production of inflammatory cytokines. J Immunol 167:3174–3181
17. **Cobb MH, Goldsmith EJ** 1995 How MAP kinases are regulated. J Biol Chem 270:14843–14846
18. **Raingeaud J, Whitmarsh AJ, Barrett T, Derijard B, Davis RJ** 1996 MKK3- and MKK6-regulated gene expression is mediated by the p38 mitogen-activated protein kinase signal transduction pathway. Mol Cell Biol 16:1247–1255
19. **Lee JC, Laydon JT, McDonnell PC, Gallagher TF, Kumar S, Green D, McNulty D, Blumenthal MJ, Heys JR, Landvatter SW** 1994 A protein kinase involved in the regulation of inflammatory cytokine biosynthesis. Nature 372:739–746
20. **Yosimichi G, Nakanishi T, Nishida T, Hattori T, Takano-Yamamoto T, Takigawa M** 2001 CTGF/Hcs24 induces chondrocyte differentiation through a p38 mitogen-activated protein kinase (p38MAPK), and proliferation through a p44/42 MAPK/extracellular-signal regulated kinase (ERK). Eur J Biochem 268:6058–6065
21. **Bhowmick NA, Zent R, Ghiassi M, McDonnell M, Moses HL** 2001 Integrin β1 signaling is necessary for transforming growth factor-β activation of p38MAPK and epithelial plasticity. J Biol Chem 276:46707–46713
22. **Kumar S, Votta BJ, Rieman DJ, Badger AM, Gowen M, Lee JC** 2001 IL-1- and TNF-induced bone resorption is mediated by p38 mitogen activated protein kinase. J Cell Physiol 187:294–303
23. **Matsumoto M, Sudo T, Saito T, Osada H, Tsujimoto M** 2000 Involvement of p38 mitogen-activated protein kinase signaling pathway in osteoclastogenesis mediated by receptor activator of NF-κB ligand (RANKL). J Biol Chem 275: 31155–31161
24. **Li X, Udagawa N, Itoh K, Suda K, Murase Y, Nishihara T, Suda T, Takahashi N** 2002 p38 MAPK-mediated signals are required for inducing osteoclast differentiation but not for osteoclast function. Endocrinology. 143:3105–3113
25. **Wong BR, Josien R, Choi Y** 1999 TRANCE is a TNF family member that regulates dendritic cell and osteoclast function. J Leukoc Biol 65:715–724
26. **Koga T, Nishihara T, Fujiwara T, Nisizawa T, Okahashi N, Noguchi T, Hamada S** 1985 Biochemical and immunobiological properties of lipopolysaccharide (LPS) from Bacteroides gingivalis and comparison with LPS from *Escherichia coli*. Infect Immun 47:638–647
27. **Suda T, Jimi E, Nakamura I, Takahashi N** 1997 Role of 1α, 25-dihydroxyvitamin D_3 in osteoclast differentiation and function. Methods Enzymol 282: 223–235
28. **Takahashi N, Yamana H, Yoshiki S, Roodman GD, Mundy GR, Jones SJ, Boyde A, Suda T** 1988 Osteoclast-like cell formation and its regulation by osteotropic hormones in mouse bone marrow cultures. Endocrinology 122: 1373–1382
29. **Inaba K, Turley S, Iyoda T, Yamaide F, Shimoyama S, Reis e Sousa C, Germain RN, Mellman I, Steinman RM** 2000 The formation of immunogenic major histocompatibility complex class II-peptide ligands in lysosomal compartments of dendritic cells is regulated by inflammatory stimuli. J Exp Med 191:927–936
30. **Baldassare JJ, Bi Y, Bellone CJ** 1999 The role of p38 mitogen-activated protein kinase in IL-1β transcription. J Immunol 162:5367–5373
31. **Rawadi G, Ramez V, Lemercier B, Roman-Roman S** 1998 Activation of mitogen-activated protein kinase pathways by Mycoplasma fermentans membrane lipoproteins in murine macrophages: involvement in cytokine synthesis. J Immunol 160:1330–1339
32. **Lu HT, Yang DD, Wysk M, Gatti E, Mellman I, Davis RJ, Flavell RA** 1999 Defective IL-12 production in mitogen-activated protein (MAP) kinase kinase 3 (Mkk3)-deficient mice. EMBO J 18:1845–1857
33. **Wang X, Studzinski GP** 2001 Inhibition of p38MAP kinase potentiates the JNK/SAPK pathway and AP-1 activity in monocytic but not in macrophage or granulocytic differentiation of HL60 cells. J Cell Biochem 82:68–77
34. **Cuenda A, Rouse J, Doza YN, Meier R, Cohen P, Gallagher TF, Young PR, Lee JC** 1995 SB 203580 is a specific inhibitor of a MAP kinase homologue which is stimulated by cellular stresses and interleukin-1. FEBS Lett 364:229–3334
35. **Enslen H, Raingeaud J, Davis RJ** 1998 Selective activation of p38 mitogen-activated protein (MAP) kinase isoforms by the MAP kinase kinases MKK3 and MKK6. J Biol Chem 273:1741–1748
36. **Young P, McDonnell P, Dunnington D, Hand A, Laydon J, Lee J** 1993 Pyridinyl imidazoles inhibit IL-1 and TNF production at the protein level. Agents Actions 39:C67–C69
37. **Prichett W, Hand A, Sheilds J, Dunnington D** 1995 Mechanism of action of bicyclic imidazoles defines a translational regulatory pathway for tumor necrosis factor α. J Inflamm 45:97–105
38. **Bachmann MF, Wong BR, Josien R, Steinman RM, Oxenius A, Choi Y** 1999 TRANCE, a tumor necrosis factor family member critical for CD40 ligand-independent T helper cell activation. J Exp Med 189:1025–1031
39. **Ishida N, Hayashi K, Hoshijima M, Ogawa T, Koga S, Miyatake Y, Kumegawa M, Kimura T, Takeya T** 2002 Large scale gene expression analysis of osteoclastogenesis in vitro and elucidation of NFAT2 as a key regulator. J Biol Chem 277:41147–41156
40. **Takayanagi H, Kim S, Koga T, Nishina H, Isshiki M, Yoshida H, Saiura A, Isobe M, Yokochi T, Inoue J, Wagner EF, Mak TW, Kodama T, Taniguchi T** 2002 Induction and activation of the transcription factor NFATc1 (NFAT2) integrate RANKL signaling in terminal differentiation of osteoclasts. Dev Cell 3:889–901

0013-7227/03/$15.00/0
Printed in U.S.A.

Endocrinology 144(12):5441–5449

doi: 10.1210/en.2003-0717

Osteoprotegerin Regulates Bone Formation through a Coupling Mechanism with Bone Resorption

MIDORI NAKAMURA, NOBUYUKI UDAGAWA, SACHIKO MATSUURA, MAKIO MOGI, HIROSHI NAKAMURA, HIROSHI HORIUCHI, NAOTO SAITO, B. YUKIHIRO HIRAOKA, YASUHIRO KOBAYASHI, KUNIO TAKAOKA, HIDEHIRO OZAWA, HIROO MIYAZAWA, AND NAOYUKI TAKAHASHI

Departments of Pediatric Dentistry (M.N., H.N., H.M.), Biochemistry (N.U.), and Oral Histology (S.M., H.O.), Institute for Oral Science (B.Y.H., Y.K., H.O., H.M., N.T.), Matsumoto Dental University, Nagano 399-0781, Japan; Department of Pharmacology, Aichi Gakuin University School of Dentistry (M.M.), Nagoya 464-8650, Japan; Department of Orthopedic Surgery, Shinshu University School of Medicine (H.H., N.S.), Nagano 399-0781, Japan; and Department of Orthopedic Surgery, Osaka City University School of Medicine (K.T.), Osaka 545-8585, Japan

Deficiency of osteoprotegerin (OPG), a soluble decoy receptor for receptor activator of nuclear factor-κB ligand (RANKL), in mice induces osteoporosis caused by enhanced bone resorption, but also accelerates bone formation. We examined whether bone formation is coupled with bone resorption in OPG-deficient ($OPG^{-/-}$) mice using risedronate, an inhibitor of bone resorption. Histomorphometric analysis showed that bone formation-related parameters (*e.g.* mineral apposition rate and osteoblast surface/bone surface) in $OPG^{-/-}$ mice sharply decreased with suppression of bone resorption by daily injection of risedronate for 30 d. $OPG^{-/-}$ mice exhibited high serum alkaline phosphatase activity and osteocalcin concentration, both of which were decreased to the levels in wild-type mice by the risedronate injection. Serum levels of RANKL were markedly elevated in $OPG^{-/-}$ mice, but were unaffected by risedronate. The ectopic bone formation induced by bone morphogenetic protein-2 implantation into $OPG^{-/-}$ mice was not accelerated even with a high turnover rate of bone, but attenuation of mineral density from the ectopic bone was more pronounced than that in wild-type mice. These results suggest that bone formation is coupled with bone resorption at local sites in $OPG^{-/-}$ mice, and that serum RANKL levels do not reflect this coupling. (*Endocrinology* 144: 5441–5449, 2003)

BONE IS continuously destroyed and reformed to maintain bone volume and calcium homeostasis in vertebrates throughout the life span. Osteoclasts and osteoblasts are specialized cells responsible for bone resorption and formation, respectively (1). In normal bone remodeling, osteoblastic bone formation follows osteoclastic bone resorption and occurs in a precise and quantitative manner. In this coupling between bone resorption and bone formation, a coupling factor that induces bone formation is assumed to be released during osteoclastic bone resorption (2). However, neither the characteristics nor the action mechanism of this coupling factor have been clarified.

The discovery of a receptor activator of nuclear factor-κB ligand (RANKL) helps elucidate the mechanisms of osteoclast differentiation and function that are regulated by osteoblasts (3–5). Osteoprotegerin (OPG), a soluble decoy receptor of RANKL, inhibits both differentiation and function of osteoclasts by inhibiting the interaction between RANKL and RANK (the receptor of RANKL) (3–5). OPG-deficient ($OPG^{-/-}$) mice exhibited severe osteoporosis due to enhanced osteoclastogenesis as adults (6, 7). Compared with wild-type (WT) mice, adult $OPG^{-/-}$ mice had lower bone mineral density (BMD), characterized by severe trabecular and cortical bone porosity, marked thinning of parietal bones of the skull, and a high incidence of fractures (6, 7). Despite this lower density, osteoblastic bone formation was higher, and serum alkaline phosphatase (ALP) activity was elevated in $OPG^{-/-}$ mice (6). These results suggest that bone formation is coupled with bone resorption in $OPG^{-/-}$ mice.

Juvenile Paget's disease, an autosomal recessive osteopathy, is characterized by rapidly remodeling woven bone, osteopenia, fractures, and progressive skeletal deformity. A homozygous deletion of the gene encoding OPG was found in two Navajo patients with juvenile Paget's disease (8). Serum ALP activities and RANKL of these patients were significantly much higher than age-matched control values (8). Thus, OPG is a critical regulator of postnatal skeletal development and homeostasis in humans as well as mice. Mutations of RANK that cause an increase in RANK-mediated nuclear factor-κB signaling *in vitro* have been found in patients suffering from familial expansile osteolysis and familial Paget's disease of bone (9). The homozygous deletion of an aspartate residue from OPG, which induces loss of function, causes an idiopathic hyperphosphatasia with high bone turnover (10). These results suggest that excessive RANKL-RANK signaling leads to a high turnover state of bone with stimulated osteoblastic bone formation. Lam *et al.* (11) also reported that RANKL increased anabolic bone formation *in vivo* when administered as an amino-terminal glutathione-*S*-transferase fusion protein into mice, suggesting that soluble RANKL in serum might be involved in the high bone turnover.

Bisphosphonates, compounds with a carbon-substituted

Abbreviations: ALP, Alkaline phosphatase; BMD, bone mineral density; OPG, osteoprotegerin; RANKL, receptor activator of nuclear factor-κB ligand; rh, recombinant human; WT, wild-type.

pyrophosphate structure (P-C-P), inhibit osteoclastic bone resorption *in vivo* and *in vitro* (12). Accumulated studies revealed the action mechanism of bisphosphonates as follows: 1) bisphosphonates bind rapidly and tightly to bone mineral when administered *in vivo* (13); 2) osteoclasts incorporate bisphosphonates during bone resorption (12–14); and 3) the incorporated bisphosphonate disrupts the cytoskeleton and induces apoptosis of osteoclasts (14, 15). Thus, bisphosphonates inhibit osteoclast function directly and specifically.

Bone morphogenetic proteins (BMPs) induce ectopic bone formation when implanted into muscular tissues (16). We have shown that phosphodiesterase inhibitors, such as pentoxifyline and rolipram, stimulated the recombinant human BMP-2 (rhBMP-2)-induced ectopic bone formation (17, 18). When phosphodiesterase inhibitors were injected into mice bearing rhBMP-2-containing implants, both the size and the mineral content in the ectopic bones induced by rhBMP-2 were higher in the inhibitor-treated mice than in control mice (17, 18). These results suggest that stimulatory or inhibitory circulating factors for bone formation in mice can be detected using a system of rhBMP-2-induced ectopic bone formation.

In the present study we examined whether bone formation is coupled with bone resorption in $OPG^{-/-}$ mice by injecting the mice daily with risedronate, a bisphosphonate, for 30 d. Histomorphometric and histochemical analyses were then performed on the femurs and vertebrae. Concentrations of serum calcium, phosphorous, osteocalcin, OPG, RANKL, and the complex of OPG and RANKL were measured. To determine whether a coupling factor is a systemic factor, circulating factors for bone formation were also examined in $OPG^{-/-}$ mice using a system of rhBMP-2-induced ectopic bone formation. When risedronate was daily injected into $OPG^{-/-}$and WT mice for 30 d, bone formation-related parameters (*e.g.* mineral apposition rate and osteoblast surface/bone surface) were sharply decreased with the suppression of osteoclastic bone resorption in $OPG^{-/-}$ mice. However, ectopic bone formation was similarly induced by the implantation of rhBMP-2 in $OPG^{-/-}$ and WT mice. The serum concentration of RANKL was markedly elevated in $OPG^{-/-}$ mice, but was unaffected by the administration of risedronate. These results suggest that bone formation is tightly coupled with bone resorption at local sites in $OPG^{-/-}$ mice, and that serum levels of RANKL do not reflect the coupling.

Materials and Methods

Animals and drugs

Male $OPG^{-/-}$, $OPG^{+/-}$ (heterozygote), and WT mice (C57BL/6J) were obtained from Japan Clea Co. (Tokyo, Japan). All procedures for animal care were approved by the animal management committee of Matsumoto Dental University. Risedronate was supplied by Procter and Gamble Pharmaceuticals (Cincinnati, OH). Other chemicals and reagents were of analytical grade.

Bone histomorphometry

Zero (saline solution alone) or 0.01 mg risedronate/kg body weight·d was sc injected into $OPG^{-/-}$ (14-wk-old), $OPG^{+/-}$ (6-wk-old), and WT (14-wk-old) mice daily for 30 d (11 animals/group). Tetracycline hydrochloride (Sigma-Aldrich Corp., St. Louis, MO; 30 mg/kg body weight) and calcein (Sigma-Aldrich Corp.; 6 mg/kg body weight) were injected on d 26 and 28, respectively, for *in vivo* fluorescent labeling of mineralization sites. Nine mice of each group were killed on d 30 for bone histomorphometric analysis. Their femurs and vertebrae were then removed, fixed in 70% ethanol, and embedded in glycol-methacrylate without decalcification. Sections were prepared and stained with Villanueva Goldner to discriminate between mineralized and unmineralized bone and to identify cellular components. Quantitative histomorphometric analysis was performed in a blind fashion. Images were also visualized by fluorescent microscopy. Nomenclature and units were used according to the recommendation of the nomenclature committee of the American Society for Bone and Mineral Research (19).

Tissue preparation for the histological analysis of bone

Two mice from each group were anesthetized with Ketalar (Sankyo, Tokyo, Japan) and were perfused for 15 min with 4% paraformaldehyde in 0.1 M phosphate buffer (pH 7.3) through the left ventricle on d 30. Femurs were removed and immersed immediately in the same fixative for an additional 20 h at 4 C. After specimens were washed with phosphate buffer, they were decalcified in 10% EDTA-2Na in 0.1 M Tris buffer (pH 7.3) for 3–4 wk at 4 C. Decalcified specimens were then washed in phosphate buffer, dehydrated in a graded series of ethanol, and embedded in semi-water-soluble resin (Immuno-Bed kit, Polysciences, Inc., Warrington, PA). Tartrate-resistant acid phosphatase, a marker enzyme of osteoclasts, was detected using enzyme histochemistry with naphthol AS-MX phosphate (Sigma-Aldrich Corp.) as a substrate and Fast Violet LB salt (Sigma-Aldrich Corp.) as a dye as previously described (7, 20).

Measurements of serum calcium, phosphorous, and osteocalcin

Blood from 18-wk-old male $OPG^{-/-}$ mice and WT mice with or without risedronate treatment was collected by heart puncture under anesthesia with diethylether. Serum concentrations of calcium and phosphorus were measured using a calcium E kit (Wako, Osaka, Japan) and an inorganic phosphorus C kit (Wako), respectively. Serum ALP activity was determined by the method of Woltgens *et al.* (21) with a slight modification as described previously (22). The amount of osteocalcin in serum was measured using a sensitive ELISA kit (Biomedical Technologies, Inc., Stoughton, MA).

Measurements of serum OPG, RANKL, and the complex of OPG and RANKL

Serum concentrations of OPG and RANKL in $OPG^{-/-}$, $OPG^{+/-}$, and WT mice treated with or without risedronate were measured using the respective ELISA kits (R&D Systems, Inc., Minneapolis, MN) as described previously (23). Serum concentrations of the complex of RANKL and OPG were also determined by the quantitative sandwich ELISA system using microplates precoated with anti-RANKL polyclonal antibodies and peroxidase-linked anti-OPG polyclonal antibodies (R&D Systems, Inc.). Quantitative analysis of the complex form of RANKL and OPG showed that RANKL bound to OPG in an equivalent molarity, and that preincubation of RANKL and OPG for 30 min at 25 C was enough to form the complex. Serum and the various concentrations of the RANKL and OPG complex were pipetted into the wells of microplates precoated with anti-RANKL polyclonal antibodies, and incubated for 12 h at 4 C to allow the binding of RANKL present in the samples to the immobilized anti-RANKL antibodies. After washing away unbound substances using PBS, peroxidase-linked polyclonal antibodies against mouse OPG were added to the wells for 2 h at room temperature. The wells were washed with PBS and then incubated with a substrate solution (tetramethylbenzidine and hydrogen peroxide) as described. The enzyme reaction yielded a blue product that turned yellow when a stop solution (1 M HCl) was added. Measurement of the complex was conducted at 450 nm using a plate reader (Biolumin 960, Amersham Pharmacia Biotech, Arlington Heights, IL). The intra- and interassay coefficients of variation were less than 11.2%.

Ectopic bone formation

rhBMP-2 was produced by Genetic Institute (Cambridge, MA) and was donated to us through Yamanouchi Pharmaceutical (Tokyo, Japan). rhBMP-2 was provided in a buffer solution (5 mM glutamic acid, 2.5%

glycine, 0.5% sucrose, and 0.01% Tween 80) at a concentration of 1 μg/μl after filter sterilization. Individual implant pellets were prepared as follows: 5 μl of the rhBMP-2 solution (1 mg/ml) were added to 20 μl 0.01 M HCl, then blotted onto a collagen sponge disk (6-mm diameter, 1-mm thickness) fabricated from commercially available bovine collagen sheets (Helistat, Integra Life Sciences Co., Plainsboro, NJ), freeze-dried as a pellet, and kept at −20 C until implantation into mice. Before the surgery for implantation, mice were anesthetized with diethylether. The pellets were implanted into the left dorsal muscle pouches (one pellet per animal) in $OPG^{-/-}$ and WT mice and then harvested after 3, 6, 9, and 12 wk. At the end of the implantation periods, the implants were harvested to evaluate size, BMD, and bone mineral content of the rhBMP-2-induced ossicle. All harvested tissues were radiophotographed with a soft x-ray apparatus (Sofron Co., Tokyo, Japan). BMD (milligrams per square centimeter) of each ossicle was measured by single energy x-ray absorptiometry using a bone mineral analyzer (DCS-600R, Aloka Co., Tokyo, Japan) (17, 18).

Statistics

Data are expressed as the mean ± SEM. Statistical analysis was performed by *t* test.

Results

Bone histomorphometry and histological analysis of bone

A previous histomorphometric study showed that osteoblastic bone formation as well as osteoclastic bone resorption were elevated in $OPG^{-/-}$ mice (6). In our current study, to examine whether bone resorption is coupled with bone formation in $OPG^{-/-}$ mice, risedronate was injected daily into $OPG^{-/-}$ mice (0.01 mg/kg body weight) for 30 d. Severe loss of trabecular bone in femora was evident in untreated 18-wk-old male $OPG^{-/-}$ mice (Fig. 1A). Treatment of $OPG^{-/-}$ mice as well as WT mice with risedronate increased the trabecular bones in the femoral neck portions (Fig. 1A). High magnification of the femoral cortical bone showed that osteoblasts of untreated $OPG^{-/-}$ mice existed as cuboidal osteoblasts along the bone surface (Fig. 1B). Risedronate treatment changed the shape of osteoblasts from cuboidal to flat. Cross-sections of femurs of untreated $OPG^{-/-}$ mice revealed excessive osteoclastic bone resorption in the endosteal sites (Fig. 1C). Risedronate treatment of $OPG^{-/-}$ mice inhibited bone resorption and increased the bone volume of femoral cortical portions. Te porous area of cortical bone was strikingly larger in untreated $OPG^{-/-}$ mice than in WT mice (Fig. 1E). Risedronate treatment of $OPG^{-/-}$ mice significantly reduced the porous area/cortical area. The double labeling study with tetracycline and calceine revealed that the width of double labels was increased in both endosteal and periosteal surfaces of cortical bones in untreated $OPG^{-/-}$ mice (Fig. 1D). Risedronate treatment narrowed this width. Bone formation rates of cortical bones in untreated $OPG^{-/-}$ mice were 2.5-fold in the endosteal surface and 1.4-fold higher in the periosteal surface than those in WT mice (Fig. 1E). Risedronate treatment of $OPG^{-/-}$ mice returned the elevated bone formation rates to those of WT mice.

Histomorphometric analysis was performed in more detail in vertebrae of $OPG^{-/-}$ and WT mice treated with or without risedronate. Most trabecular bones were lost in the vertebrae of untreated $OPG^{-/-}$ mice (Fig. 2A). Risedronate treatment markedly increased vertebral trabecular bones in $OPG^{-/-}$ mice as well as in WT mice. Bone resorption-related parameters (osteoclast surface/bone surface, osteoclast number/bone surface, and eroded surface/bone surface) were all elevated in untreated $OPG^{-/-}$ mice (Fig. 2B). Risedronate treatment significantly decreased these elevated parameters. Risedronate treatment only slightly decreased these bone resorption-related parameters in WT mice (Fig. 2B).

Similar to the osteoblasts in the cortical bones (Fig. 1B), osteoblasts along the vertebral trabecular bones of untreated $OPG^{-/-}$ mice were more cuboidal than those in WT mice (Fig. 3A). Risedronate treatment of $OPG^{-/-}$ mice changed the shape of the osteoblasts from cuboidal to flat. A double-labeling study revealed that mineralization of trabecular bones in untreated $OPG^{-/-}$ mice was markedly elevated, and treatment with risedronate apparently suppressed the mineralization of these bones, as evidenced by the disappearance of the thickly labeled surfaces (arrows in Fig. 3B). The static histomorphometric measurements showed that bone formation-related parameters (osteoid volume/bone volume, mineral apposition rate, osteoblast surface/bone surface, and bone formation rate/bone surface) were all significantly higher in untreated $OPG^{-/-}$ mice than in WT mice (Fig. 3C). Risedronate treatment decreased these elevated bone formation-related parameters to levels lower than those in WT mice. Risedronate treatment also decreased the bone formation-related parameters in WT mice (Fig. 3C). Bone volume/tissue volume and trabecular number of vertebrae were significantly lower in $OPG^{-/-}$ mice than in WT mice (Fig. 3D). Risedronate treatment increased bone volume and trabecular number in both $OPG^{-/-}$ and WT mice. These results suggest that the increase in bone resorption due to OPG deficiency is more accelerated than the compensatory increase in bone formation in $OPG^{-/-}$ mice.

Serum calcium, phosphorous, and osteocalcin

There were no significant differences in serum concentrations of calcium and phosphorus between $OPG^{-/-}$ and WT mice (Fig. 4). Serum phosphorus levels in risedronate-treated mice were significantly lower than those in WT mice (Fig. 4). Serum parameters of bone formation (ALP activity and osteocalcin concentration) were about four and three times higher, respectively, in $OPG^{-/-}$ mice than in WT mice (Fig. 4). Risedronate treatment of $OPG^{-/-}$ mice resulted in decreases in serum ALP activity and osteocalcin concentration to the levels found in WT mice.

Serum OPG, RANKL, and the complex of OPG and RANKL

Serum levels of RANKL were elevated in a patient with OPG-deficient juvenile Paget's disease (8). Furthermore, circulating RANKL stimulated anabolic bone formation *in vivo* (11). We therefore measured the serum levels of RANKL and OPG in $OPG^{-/-}$, $OPG^{+/-}$ (heterozygote), and WT mice treated with or without risedronate (Fig. 5). Although serum OPG was detectable in $OPG^{+/-}$ and WT mice, the level in $OPG^{+/-}$ mice was significantly lower than that in WT mice. The serum level of RANKL was extremely low in WT mice, but was markedly elevated in $OPG^{-/-}$ mice. The serum level of RANKL in $OPG^{+/-}$ mice was significantly higher than that in WT mice, but lower than that in $OPG^{-/-}$ mice.

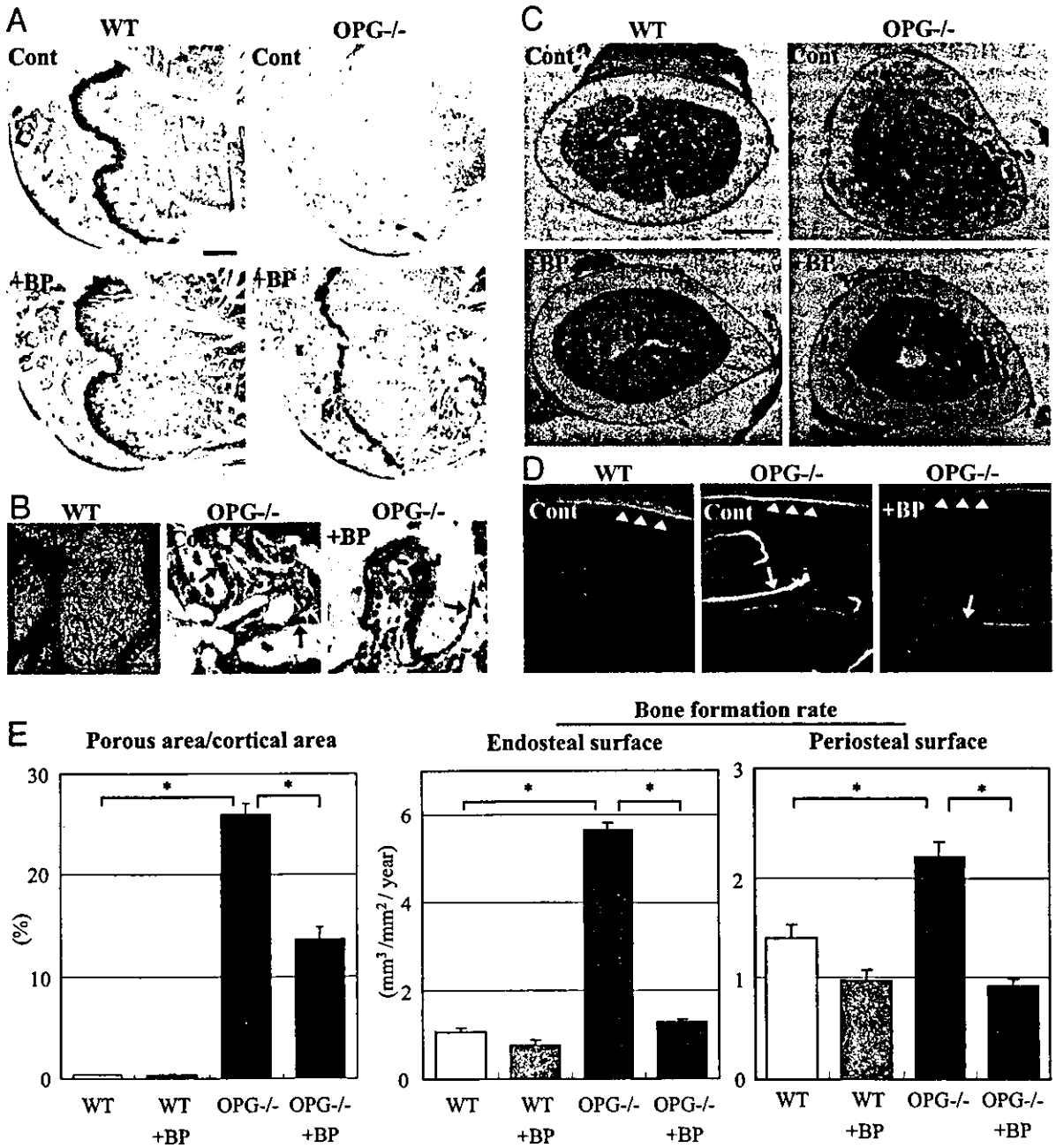

FIG. 1. Effects of risedronate treatment on femurs of $OPG^{-/-}$ and WT mice. $OPG^{-/-}$ and WT mice were injected daily with (+BP) or without (Cont) risedronate (0.01 mg/kg body weight·d) for 30 d. Mice were given interval doses of tetracycline and calceine on d 26 and 28, respectively. Femurs were removed on d 30 for histological and histomorphometric analyses. A, Histological evaluation of proximal femurs. *Bar*, 500 μm. B, High magnification of femoral cortical bones. *Arrows* indicate osteoblasts along the bone surface. Osteoblasts of $OPG^{-/-}$ mice not treated with risedronate appear more cuboidal in shape than those of WT mice or those of $OPG^{-/-}$ mice treated with risedronate. *Bar*, 50 μm. C, Cross-sections of femurs. *Bar*, 500 μm. D, Fluorescent micrographs showing double-labeled mineralization in the fronts of femurs. *Arrows* and *arrowheads* indicate endosteal and periosteal bone formation, respectively. *Bar*, 100 μm. E, Histomorphometric analysis of femurs. Parameters of bone resorption and formation were determined in femoral cortical bones. Data are expressed as the mean ± SEM of four to six animals. Statistical significance was analyzed by *t* test: *, $P < 0.0001$.

There was a possibility that OPG interfered with the interaction between anti-RANKL antibodies and RANKL in the ELISA when OPG formed a complex with RANKL in serum. Therefore, we established an ELISA for the complex of OPG-RANKL and then compared the serum levels of the complex among $OPG^{-/-}$, $OPG^{+/-}$, and WT mice (Fig. 5). The complex of OPG-RANKL in serum was detected in $OPG^{+/-}$ mice but not in WT mice (Fig. 5). Treatment of $OPG^{-/-}$, $OPG^{+/-}$, and WT mice with risedronate showed no effect on the circulating levels of RANKL, OPG, and the complex of OPG and RANKL (Fig. 5). These results suggest that circulating RANKL does not reflect the status of bone resorption and formation in $OPG^{-/-}$ mice, and that the serum concentration of RANKL is tightly regulated by circulating OPG.